

Cell-Type-Specific Recruitment of Amygdala Interneurons to Hippocampal Theta Rhythm and Noxious Stimuli In Vivo

Thomas C.M. Bienvenu,^{1,3,*} Daniela Busti,² Peter J. Magill,¹ Francesco Ferraguti,² and Marco Capogna^{1,*}

¹Medical Research Council Anatomical Neuropharmacology Unit, Department of Pharmacology, University of Oxford, Mansfield Road, Oxford OX1 3TH, UK

²Department of Pharmacology, Innsbruck Medical University, Peter Mayr Str. 1a, A-6020 Innsbruck, Austria

³Present address: INSERM U862, Neurocentre Magendie, 146 rue Léo Saignat, 33077 Bordeaux, France

*Correspondence: marco.capogna@pharm.ox.ac.uk (M.C.), thomas.bienvenu@inserm.fr (T.C.M.B.)

DOI 10.1016/j.neuron.2012.04.022

SUMMARY

Neuronal synchrony in the basolateral amygdala (BLA) is critical for emotional behavior. Coordinated theta-frequency oscillations between the BLA and the hippocampus and precisely timed integration of salient sensory stimuli in the BLA are involved in fear conditioning. We characterized GABAergic interneuron types of the BLA and determined their contribution to shaping these network activities. Using in vivo recordings in rats combined with the anatomical identification of neurons, we found that the firing of BLA interneurons associated with network activities was cell type specific. The firing of calbindin-positive interneurons targeting dendrites was precisely theta-modulated, but other cell types were heterogeneously modulated, including parvalbumin-positive basket cells. Salient sensory stimuli selectively triggered axo-axonic cells firing and inhibited firing of a distinct projecting interneuron type. Thus, GABA is released onto BLA principal neurons in a time-, domain-, and sensory-specific manner. These specific synaptic actions likely cooperate to promote amygdalo-hippocampal synchrony involved in emotional memory formation.

INTRODUCTION

Understanding how the brain processes emotions holds major potential for fundamental and medical research. Precisely timed neuronal activity across brain regions is crucial for cognitive processing (Singer, 1999). Studies in humans (Richardson et al., 2004) and rodents (Maren and Fanselow, 1995) indicate that cooperation between amygdala and hippocampus is critical for emotional memory formation. This communication involves the synchronization of neuronal activity at theta (θ) frequencies (4–10 Hz) across the basolateral amygdala complex (BLA) and the CA1 hippocampal field. In fear conditioning, a model of emotional memory, animals learn to associate a negative

emotional valence to an initially neutral stimulus (e.g., a tone) after its repetitive pairing with an aversive stimulus (e.g., an electrical footshock) (LeDoux, 2000). Unconditioned animals show hippocampus-related θ oscillations in BLA at the levels of individual principal cells and neuron populations (as reflected in local field potentials, LFPs) (Paré and Gaudreau, 1996). Amplitude and power of this rhythm increase after auditory, contextual or social fear learning (Jeon et al., 2010; Paré and Collins, 2000; Seidenbecher et al., 2003). Moreover, the degree of θ synchrony between BLA and CA1 after fear conditioning predicts memory performance (Popa et al., 2010). Precise timing of activity in the BLA is likely important not only for oscillations. It may also be critical for memory encoding, by selectively assigning emotional valence to incoming sensory stimuli. However, how BLA network activities are coordinated remains unknown.

Several lines of evidence suggest that GABAergic neurons may be instrumental in controlling θ oscillations and integrating salient sensory stimuli in the BLA. The BLA is a cortical-like area; in cortex, GABAergic interneurons can synchronize the activity of large cell assemblies (Bonifazi et al., 2009; Cobb et al., 1995). Persistent BLA θ oscillations are accompanied by fear extinction deficits in GAD65 knockout mice (Sangha et al., 2009). Furthermore, electrical footshocks evoke synchronous GABAergic currents in BLA principal neurons (Windels et al., 2010).

GABAergic cells in the BLA are comprised of several groups (McDonald, 1982; Sosulina et al., 2010), with diverse neurochemical expression profiles (Jasnow et al., 2009; Mascagni and McDonald, 2003; Rainnie et al., 2006; Smith et al., 2000). These might play specific physiological roles. However, GABAergic cell types of the BLA have not been fully characterized, and there is a pressing need to define the nature and function of such cellular diversity (Ehrlich et al., 2009). A division of labor between GABAergic cell types in controlling local network activities is exemplified in hippocampus, where cells innervating distinct neuronal compartments fire at specific oscillation phases (Klausberger et al., 2003; Tukker et al., 2007). We hypothesized that BLA GABAergic cells contribute in a type-specific manner to the coordination of θ oscillatory interactions with the hippocampus and local responses to salient sensory stimuli. We investigated this by recording the spontaneous and noxious stimulus-driven firing of anatomically-identified BLA interneurons in vivo. Our findings demonstrate that

Table 1. Spontaneous Firing of the GABAergic Interneurons Recorded In Vivo

Recorded neurons		Spontaneous Firing during dCA1 Theta					
Type	Cell Code	Rate (Hz)	CV	Mean Angle	Angular Deviation	p (Rayleigh)	Modulation Depth
Axo-axonic	tjx20f	6.5	1.41	n.s.	n.s.	1.7×10^{-1}	n.s.
	tjx27b	15.9	0.82	n.s.	n.s.	3.5×10^{-1}	n.s.
	tjx56b	7.9	1.00	187.0	137.5	2.2×10^{-6}	0.06
	tjx63a	15.6	1.02	251.5	156.0	3.7×10^{-3}	0.02
	tjx66a	13.0	1.28	213.0	127.0	4.3×10^{-41}	0.09
	tjx74a	15.4	0.97	283.7	146.5	1.1×10^{-7}	0.04
PV+ basket	tjx38a	23.1	0.66	n.s.	n.s.	5.5×10^{-3}	n.s.
	tjx41c	23.7	0.69	357.5	148.1	3.9×10^{-5}	0.04
	tjx42b	16.7	0.67	173.9	141.8	2.2×10^{-10}	0.05
	tjx43a	6.4	0.93	n.s.	n.s.	1.4×10^{-1}	n.s.
	tjx48a	27.2	0.61	14.7	150.2	1.9×10^{-7}	0.03
	tjx49a	3.9	1.18	83.2	133.7	4.0×10^{-8}	0.07
	tjx53a	6.8	1.97	150.1	163.9	3.2×10^{-3}	0.02
	tjx55b	9.4	1.03	13.2	113.3	3.7×10^{-44}	0.14
	tjx61a	8.6	1.25	125.1	141.7	5.1×10^{-8}	0.05
	tjx69a	12.2	0.94	136.5	156.7	1.4×10^{-4}	0.02
	tjx72b	4.3	1.27	140.8	146.2	1.5×10^{-5}	0.04
	tjx72d	1.8	1.28	97.8	130.2	1.3×10^{-6}	0.08
	tjx78a	6.2	0.97	339.9	108.4	4.1×10^{-38}	0.17
	tjx86b	10.4	0.96	n.s.	n.s.	1.5×10^{-2}	n.s.
tjx87b	4.9	1.00	183.5	145.5	5.7×10^{-9}	0.04	
CB+ dendrite-targeting	tjx21i	4.3	0.96	145.0	127.5	5.1×10^{-13}	0.08
	tjx22c	3.1	1.00	145.5	112.9	1.8×10^{-31}	0.14
	tjx59b	3.0	1.03	144.3	110.6	6.8×10^{-20}	0.16
AStria-projecting	tjx45a	3.4	1.54	n.s.	n.s.	7.9×10^{-1}	n.s.
	tjx52a	6.0	1.15	155.7	111.5	3.6×10^{-42}	0.15
	tjx68a	4.1	0.98	158.2	122.0	7.3×10^{-13}	0.10
	tjx83c	4.6	1.60	284.9	122.9	6.3×10^{-10}	0.10

CV: coefficient of variation of interspike intervals (variance/mean); n.s.: not statistically significant.

distinct types of BLA GABAergic cell fulfill specialized and complementary roles in regulating behaviorally relevant network activities.

RESULTS

We simultaneously recorded spontaneous single-neuron activity in BLA (comprised of the lateral and basal nuclei) and hippocampal θ oscillations in dorsal CA1 (dCA1) LFPs of urethane-anesthetized rats. Prominent θ oscillations (4.15 ± 0.23 Hz, mean \pm SD) occurred during cortical activated states in dCA1 (Klausberger et al., 2003), but not in BLA LFPs. Gamma (γ) oscillations were also detected in dCA1 LFPs (42.1 ± 1.60 Hz, mean \pm s.d.).

We recorded interneuron responses to noxious stimuli by delivering electrical shocks and pinches to the hindpaw contralateral to the recording sites. We also examined the firing of BLA glutamatergic principal neurons in relation to dCA1 θ . After recordings, neurons were juxtacellularly filled with Neurobiotin, allowing for their unambiguous identification.

Interneurons with somata in the BLA were recorded and labeled (Figure S1, available online, shows cell locations). These were GABAergic, as all tested cells expressed the vesicular GABA transporter (VGAT) and/or glutamate decarboxylase (GAD; Figures 3F and 4I), and all synapses examined with electron microscopy were symmetric. Interneuron types were distinguished according to the combination of their postsynaptic targets, neurochemical markers and axo-dendritic patterns. Twenty eight GABAergic cells could be classified in four types: axo-axonic, parvalbumin-expressing basket, calbindin-expressing dendrite-targeting, and "AStria-projecting" cells.

Axo-Axonic Cells Increase Their Firing in Response to Noxious Stimuli

Axo-axonic cells ($n = 6$) were recorded and anatomically identified. During dCA1 θ , they spontaneously fired action potentials at a mean frequency of 12.4 Hz (range 6.5–15.9 Hz; Table 1; Figure 1A). The firing of 4 of 6 cells was significantly modulated in phase with dCA1 θ ($p < 0.005$, Rayleigh test), albeit weakly (mean modulation depth (r) = 0.05, see Experimental

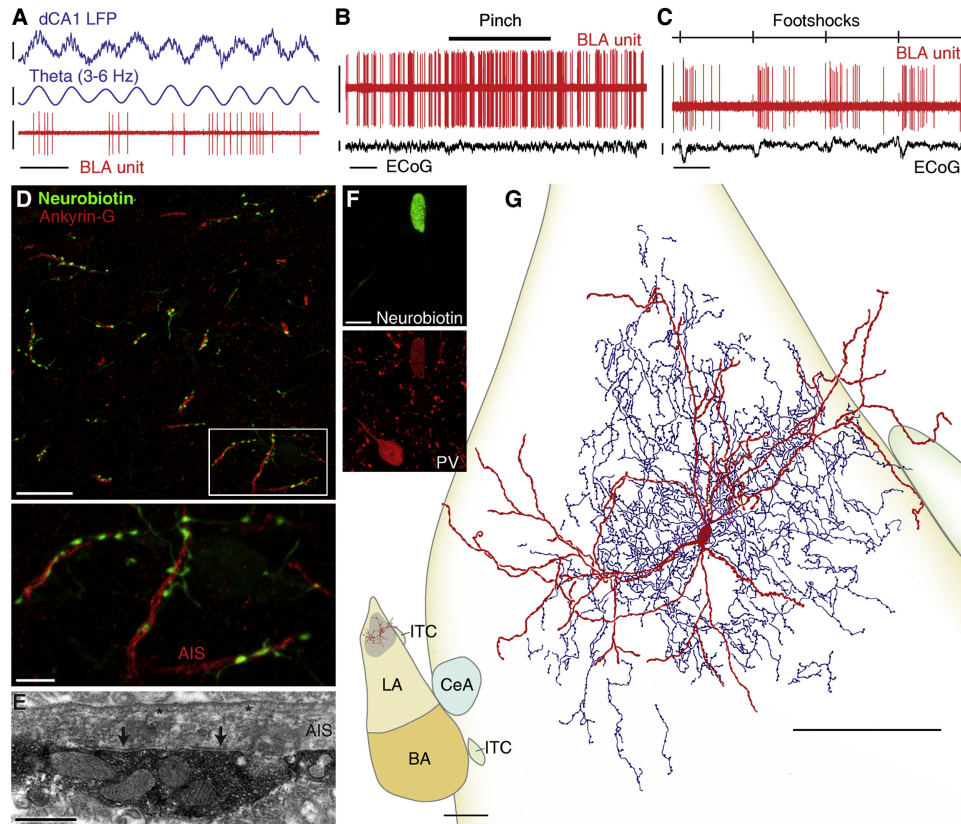


Figure 1. Axo-axonic Cells: Firing In Vivo and Anatomical Characterization

(A) In vivo, the neuron tjx20f fired non θ -modulated spike trains.

(B) tjx20f increased its firing rate in response to hindpaw pinches. The electrocorticogram (ECoG) shows stable global activation.

(C) Another representative axo-axonic cell (tjx56b), dramatically increased firing upon hindpaw electrical shocks.

(D) Close appositions between tjx63a axon varicosities and ankyrin G-expressing axon initial segments (AIS). Low (top) and high magnification (of area delineated, bottom) of projection of a confocal z stack of 4.42 μ m thickness.

(E) Electron micrograph of a DAB-labeled axon bouton (tjx20f) forming two synaptic junctions (arrows) with a single AIS. *undercoating.

(F) tjx20f is immunopositive for parvalbumin (PV; single confocal optical section).

(G) Reconstruction of tjx20f. Soma and entire dendritic tree (red) are drawn from 5 sections of 60 μ m thickness. Axon (blue, main axon is purple) is drawn from 2 sections, for clarity. Inset: position of tjx20f dendrites (in red) in the BLA and axonal field extent (gray area) estimated from the two drawn and surrounding sections. Boundary colors apply to the main panel. LA: lateral amygdala, BA: basal amygdala, CeA: central amygdala, ITC: intercalated cells cluster. Orientation: top: dorsal, right: medial.

Scale bars: (A) LFP raw and filtered: 0.4 mV, unit: 1 mV, time: 400 ms; (B) unit: 1 mV, ECoG: 0.25 mV, time: 4 s; (C) unit: 1 mV, ECoG: 0.25 mV, time: 1 s; (D) top: 20 μ m, bottom: 5 μ m; (E) 500 nm; (F) 10 μ m; (G) 100 μ m, inset 500 μ m. See also Figures S1–S5 and Tables S1–S3.

Procedures). Two cells fired independently from the hippocampal θ rhythm (Figure 1A). The four θ -modulated cells fired preferentially between the peak and the descending phase of dCA1 θ (range 187.0–283.7°, where 0° and 360° represent θ troughs; θ phase histograms of single neurons are illustrated in Figure S2). However, statistical analysis showed that these four cells did not form a synchronized population in relation to dCA1 θ ($R' = 1.03$, $R_{0.05,4} = 1.09$, Moore test). Furthermore, the firing of axo-axonic cells did not show statistically significant modulation in phase with dCA1 γ oscillations ($p > 0.1$, Rayleigh test, $n = 6$; Figure S3; Table S3).

Axo-axonic cells displayed dramatic short-latency excitations in response to noxious stimuli. All axo-axonic cells increased their firing rates upon hindpaw pinches (+377% of baseline, latency 267 ms, peak 377 ms, $n = 6$; ranges: 133%–606%,

latency 200–400 ms, peak 400–600 ms, respectively; Table 2; individual histograms are shown in Figure S4). This excitation rapidly adapted, and was curtailed at stimulus offset (Figure 5D). Responses to electrical footshocks were similarly pronounced (mean 226% of baseline, latency 50 ms, peak 225 ms, $n = 4/4$; ranges 133%–606%, 20–100 ms, 20–420 ms, respectively; Figure 1C; Table 2; individual histograms, Figure S5).

These neurons exhibited typical axo-dendritic patterns. Their axons formed cartridges. Almost all of large-axon varicosities were in close apposition with ankyrin G-expressing axon initial segments, ($n = 6/6$ cells), as seen with immunofluorescence (Figure 1D). We analyzed randomly-sampled synapses from two of these cells using electron microscopy. The vast majority of post-synaptic targets were axon initial segments (95.4%, $n = 43$ synapses; Figure 1E; Table S1), confirming that these cells

Table 2. Noxious Stimulus-Driven Firing of the GABAergic Interneurons

Recorded Neurons		Hindpaw Pinch Responses				Electrical Footshock Responses			
Type	Cell Code	Response	Latency (ms)	Peak (ms)	%	Response	Latency (ms)	Peak (ms)	%
Axo-axonic	tjx20f	E	200	600	378	n.t.	n.t.	n.t.	n.t.
	tjx27b	E	200	400	305	E	40	260	299
	tjx56b	E	200	400	606	E	100	200	194
	tjx63a	E-I	200-1120	600-1120	133-100	n.t.	n.t.	n.t.	n.t.
	tjx66a	E	400	600	595	E	40	420	239
	tjx74a	E	400	400	246	E-I-E	20-40-140	20-60-220	172-81-213
PV+ basket	tjx38a	E	1200	2800	125	n.t.	n.t.	n.t.	n.t.
	tjx41c	I	9600	9800	55	I	100	100	38
	tjx42b	E-I	200-1040	200-1060	130-72	I	100	240	45
	tjx43a	n.t.	n.t.	n.t.	n.t.	n.t.	n.t.	n.t.	n.t.
	tjx48a	I	5000	5000	27	E	20	20	71
	tjx49a	E	600	2400	218	n.s.	n.s.	n.s.	n.s.
	tjx53a	n.s.	n.s.	n.s.	n.s.	E	20	100	115
	tjx55b	E	200	8800	526	I	180	220	68
	tjx61a	E	600	1600	153	n.s.	n.s.	n.s.	n.s.
	tjx69a	E-I	200-1600	200-2800	160-100	n.s.	n.s.	n.s.	n.s.
	tjx72b	I	5000	5000	100	I	340	400	100
	tjx72d	n.t.	n.t.	n.t.	n.t.	n.t.	n.t.	n.t.	n.t.
	tjx78a	E	600	600	314	E	40	180	170
	tjx86b	E	2200	2200	62	n.t.	n.t.	n.t.	n.t.
	tjx87b	n.t.	n.t.	n.t.	n.t.	I	100	200	72
CB+ dendrite-targeting	tjx21i	I	4200	4400	100	n.t.	n.t.	n.t.	n.t.
	tjx22c	n.t.	n.t.	n.t.	n.t.	n.t.	n.t.	n.t.	n.t.
	tjx59b	n.s.	n.s.	n.s.	n.s.	n.t.	n.t.	n.t.	n.t.
AStria-projecting	tjx45a	I	1000	1000	100	I	60	740	100
	tjx52a	I	1600	1800	100	n.t.	n.t.	n.t.	n.t.
	tjx68a	n.s.	n.s.	n.s.	n.s.	I	20	20	75
	tjx83c	I	3800	3800	100	I	20	380	81

%; maximal percentage of sensory-evoked firing changes; E: excitation; I: inhibition; n.s.: not statistically significant; n.t.: not tested.

were of the axo-axonic type. All axo-axonic cells expressed parvalbumin (PV), sometimes weakly (Figure 1F), but were never calbindin (CB)-positive. Two of 6 neurons densely expressed the GABA_AR- α 1 subunit on their dendrites (immunohistochemical results are summarized in Table S2). Axo-axonic cells were bi-tufted. Their dendrites did not branch immediately, were tortuous and sparsely spiny (Figure 1G). Axonal arborizations of all 6 cells were very dense and mostly contained within the dendritic field. Axons were always restricted to the BLA, but could be distributed between lateral and basal nuclei.

These results show that the firing of axo-axonic cells of the BLA dramatically increases in response to salient sensory stimuli. However, their spontaneous population activity is not tightly synchronized with hippocampal θ (Figure 5).

Parvalbumin-Expressing Basket Cell Assemblies Tonicly Inhibit Principal Cells

Next, we studied the firing of parvalbumin-expressing (PV⁺) basket cells ($n = 15$). During dCA1 θ oscillations, PV⁺ basket cells fired at a mean frequency of 11.0 Hz (range 1.8–27.2 Hz; Table 1),

some tonically (coefficient of variation (CV) < 1, $n = 8/15$), others irregularly (CV > 1, $n = 7/15$). It has been frequently speculated that PV⁺ basket cells pace θ rhythms in the BLA (reviewed in Ehrlich et al., 2009). Instead, we found that most cells were only weakly modulated with dCA1 θ (mean $r = 0.06$; Figure 2A), and at dispersed phases (Table 1; Figures 5B and S2). In keeping with this, the firing of PV⁺ basket cells as a population was not synchronized with this rhythm ($R^2 = 0.73$, $R_{0.05,12} = 1.042$, Moore test; Figure 5A). The firing of PV⁺ basket cells was not modulated with dCA1 γ oscillations ($p > 0.04$, Rayleigh test, $n = 15$; Figure S3; Table S3).

As with θ modulation, PV⁺ basket cells displayed heterogeneous and generally moderate responses to noxious stimuli (Figure 2B; Table 2). Half of the cells tested (6/12) were excited by hindpaw pinches, three were inhibited, two showed an excitation-inhibition sequence, and one cell did not respond significantly (Figure S4). Several cells tested (5/11) were inhibited by electrical footshocks, three cells were excited, and three other cells did not change their firing rates (Figure S5). Cells that were excited in response to one type of noxious stimulus could be

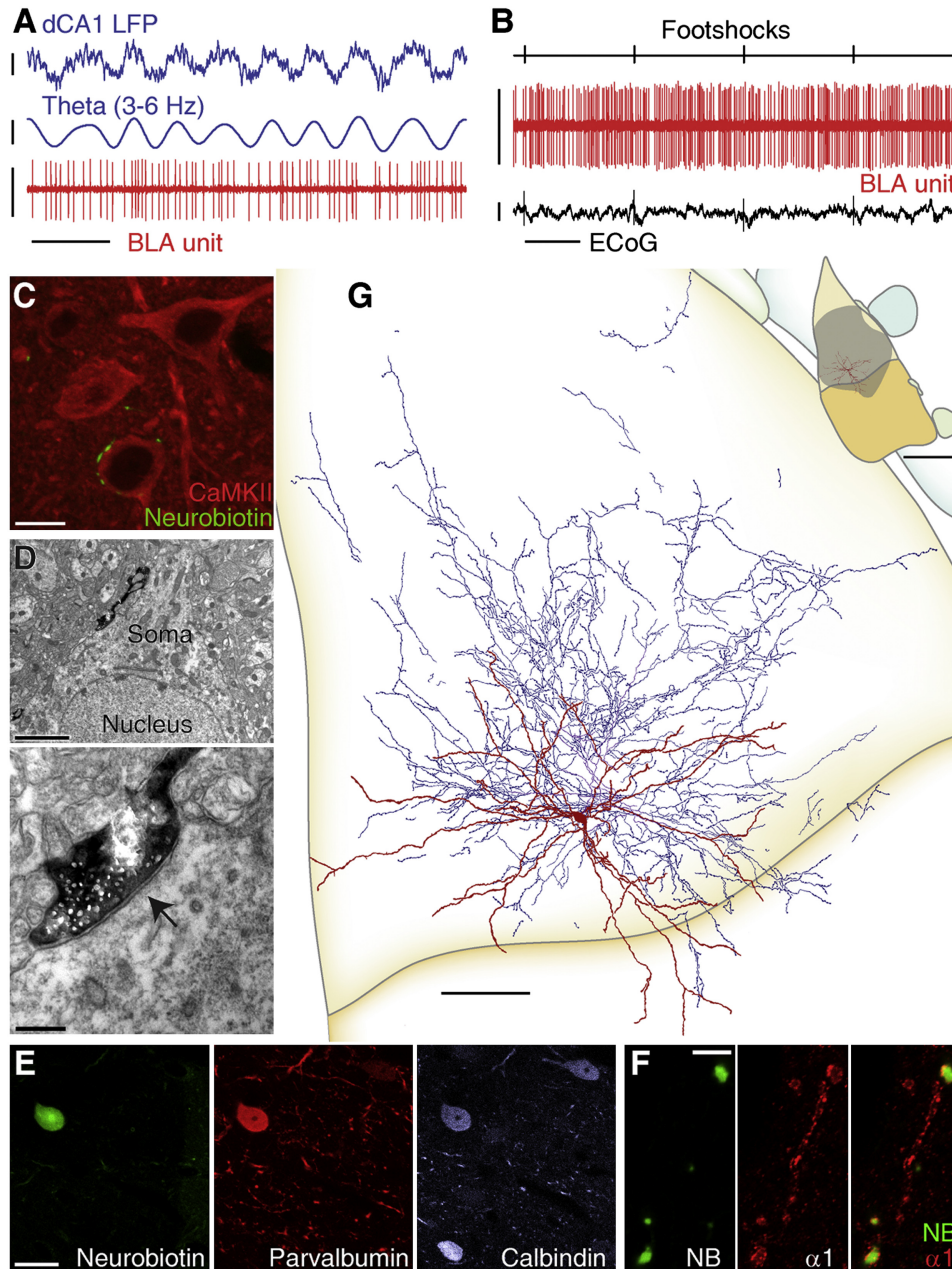


Figure 2. PV Basket Cells: Firing In Vivo and Anatomical Characterization

All panels show data from the same neuron (txj48a).

(A) Tonic, weakly modulated firing during hippocampal θ oscillations.

(B) Moderate firing increases in response to hindpaw electrical shocks, not noticeable in the raw data.

(C) Axon varicosities making close appositions with the soma of a CaMKII α^+ principal neuron (projection of a confocal z stack of 3.29 μm thickness).

(D) Low (top) and high magnification (bottom) electron micrographs of a synapse (arrow) made by a labeled axon bouton with a soma.

(E) Immunopositivity for parvalbumin and calbindin. Immunofluorescence confocal images (single optical section).

(F) Accumulation of GABA $_A$ R- $\alpha 1$ ($\alpha 1$) at the dendritic membrane of the Neurobiotin (NB)-filled cell (single confocal optical sections).

(G) Reconstruction of txj48a. Soma and entire dendritic tree are drawn from 12 sections of 60 μm thickness. Axon is drawn from 2 sections for clarity. Inset: position of txj48a dendrites in the BLA and axonal field extent estimated from the two drawn and surrounding sections (color code as in Figure 1G). Orientation: top: dorsal, right: medial.

Scale bars: (A) LFP raw and filtered: 0.4 mV, unit: 1 mV, time: 400 ms; (B) unit: 1 mV, ECoG: 0.25 mV, time: 1 s; (C) 10 μm ; (D) top 2 μm , bottom 250 nm; (E) 20 μm ; (F) 5 μm ; (G) 100 μm , inset 500 μm . See also Figures S1–S7 and Tables S1–S3.

inhibited by the other stimulus (Table 2). This further shows that the firing of PV⁺ basket cells is not selectively tuned by noxious stimuli. Importantly, heterogeneous firing among PV⁺ basket cells does not reflect spatial segregation of activity patterns in the BLA (see Figure S1A and Table 1).

Axon varicosities of these cells were large and clustered. Light microscopic analysis (n = 12 cells) revealed that they mostly made close appositions with somata and large dendrites of BLA neurons expressing the calcium/calmodulin-dependent kinase II alpha subunit (CaMKII α ; Figure 2C), a marker of principal cells (Supplemental Experimental Procedures). Electron microscopic analysis confirmed that the main postsynaptic targets were somata (55%; n = 40 synapses, 2 cells; Figures 2D and S6C) and proximal dendrites (45%; diameter 1.29 \pm 0.1 μ m; Figures S6A and S6B; Table S1). For 72.5% of these synapses, the postsynaptic target was unambiguously identified as a CaMKII α principal neuron (Figures S6A and S6C, Table S1). Thus, our results established that these interneurons were basket cells.

In addition to PV, these cells always expressed CB and an accumulation of the GABA_AR- α 1 subunit along their somatodendritic plasma membranes (n = 12/12 cells; Figures 2E and 2F; Table S2). This neurochemical pattern is distinct from those of the other cell types studied here. Three PV⁺ neurons were classified as basket cells based on these features, although their axons could not be analyzed. In addition, PV⁺ basket cells displayed characteristic axonal and dendritic fields. They were multipolar. Their dendrites were varicose, typically aspiny, straight, and branched rarely (Figure 2G). Axonal arborizations were dense within the dendritic field and extended beyond it in radial branches, sometimes over long ranges (Figure S7A). This suggests that some PV⁺ basket cells influence neuronal activities in large parts of the BLA. Overall, PV⁺ basket cells show distinct postsynaptic targets and neurochemical contents, demonstrating they are different cell types in the BLA.

As a group, PV⁺ basket cells do not appear to fire tuned to dCA1 θ or noxious stimuli (Figure 5). Thus, assemblies of them may tonically inhibit principal neurons. The finding that axo-axonic and PV⁺ basket cell groups do not fire in synchrony with hippocampal θ rhythm raises the question of which interneurons might fulfill this role.

Calbindin-Expressing Dendrite-Targeting Cells Fire Synchronously with Hippocampal Theta Oscillations

Dendrite-targeting CB⁺ cells spontaneously fired at a mean frequency of 3.5 Hz (range 3.0–4.3 Hz, n = 3; Table 1). Their firing was consistently and strongly modulated with the late ascending phase of dCA1 θ (Figure 3A; mean angle 144.9°, mean r = 0.13; Figures 5B and S2; Table 1). Thus, as a population, CB⁺ dendrite-targeting cells did fire tightly synchronized with hippocampal θ (R' = 1.15, $R_{0.05,3}$ = 1.095, p < 0.05, Moore test; Figure 5A). In contrast, none of these cells fired in phase with dCA1 γ (p > 0.1, Rayleigh test, n = 3; Figure S3; Table S3).

Responses to hindpaw pinches could be tested in two cells. One cell did not significantly change its firing (Figure 3B); the other was inhibited (latency 4.2 s, peak 4.4 s; Table 2; Figure S4). Electrical footshocks were applied during recording of the third cell. In this experiment, only 53 shocks were applied and

no change in firing was observed. Such a sample size is a limitation of the juxtacellular recording/labeling technique used. It cannot be ruled out that more heterogeneous activity relationships with θ oscillations or sensory stimuli would emerge if a larger sample of CB⁺ cells were available.

When examined with light microscopy, axons of the three cells were distributed in the BLA neuropil. Some axon varicosities made close appositions with dendrites of CaMKII α ⁺, principal neurons. A substantial proportion was not in apposition with identifiable CaMKII α ⁺ structures (Figure 3C) and likely contacted small dendritic processes that could not be resolved with light microscopy. Electron microscopic analysis demonstrated that postsynaptic targets were exclusively dendrites of small to medium diameter (0.59 \pm 0.05 μ m, n = 41 synapses, 2 cells; Figure 3D; Table S1). Notably, this diameter value was the smallest among the neuron types studied (p < 0.05, Kruskal-Wallis test with Dunn's multiple comparison; Figure S6E). In 24% of these synapses, targets were confirmed to be CaMKII α ⁺ dendrites of principal neurons (Figure 3D).

In addition to strongly expressing CB (Figure 3E), two neurons tested contained very low levels of PV in their somata (but no detectable PV in their dendrites). One cell was GABA_AR- α 1⁺. The cells were immunonegative for other molecules tested, including somatostatin (Table S2). Dendrites emerged in bipolar arrangement from the soma. They were tortuous, rough, and sometimes spiny. Axons and dendrites were restricted to the BLA, but could span lateral and basal nuclei (Figure 3G).

These results show that CB⁺ dendrite-targeting cells represent a specific cell type, whose firing is synchronized with CA1 θ (Figure 5A).

Amygdalo-striatal Transition Area-Projecting Neurons Are Inhibited by Noxious Stimuli

We discovered a GABAergic cell type that projects to the amygdalo-striatal transition area (ASTria, hence its name), as well as innervating the BLA (Figures 4C and S7B). The firing of most ASTria-projecting cells (mean frequency 4.01 Hz, range 3.4–6.0 Hz, n = 4; Table 1) was related to dCA1 θ (n = 3/4, mean r = 0.12). Two of these cells preferentially fired before the peak (Figure 4A) and one fired most during the descending phase of the θ rhythm (Figures 5B and S2; Table 1). As a result, this cell population was not statistically phase-locked to hippocampal θ (R' = 0.86, $R_{0.05,3}$ = 1.095, Moore test). The firing of ASTria-projecting neurons was not modulated with dCA1 γ oscillations (p > 0.04, Rayleigh test, n = 4; Figure S3; Table S3).

In contrast to the previous three cell types, ASTria-projecting cells were robustly inhibited by noxious stimuli. Hindpaw pinches suppressed the firing of 3/4 cells tested (Figure 4B; mean latency 2,133 ms, peak 2,200 ms; ranges, 1,000–3,800 ms for peak and latency; Table 2; Figure S4). In two cells, this inhibition persisted for several seconds after the pinch offset (Figure 5D). Electrical footshocks also elicited strong inhibitory responses in ASTria-projecting cells (–85% of baseline, latency 33 ms, peak 380 ms, n = 3; ranges: 75%–100%, 20–60 ms, 20–740 ms, respectively; Figures S5 and 5C).

The axon projecting to the ASTria innervated somata and dendrites of DARPP-32⁺ cells, likely medium-sized spiny neurons (Anderson and Reiner, 1991), which also expressed

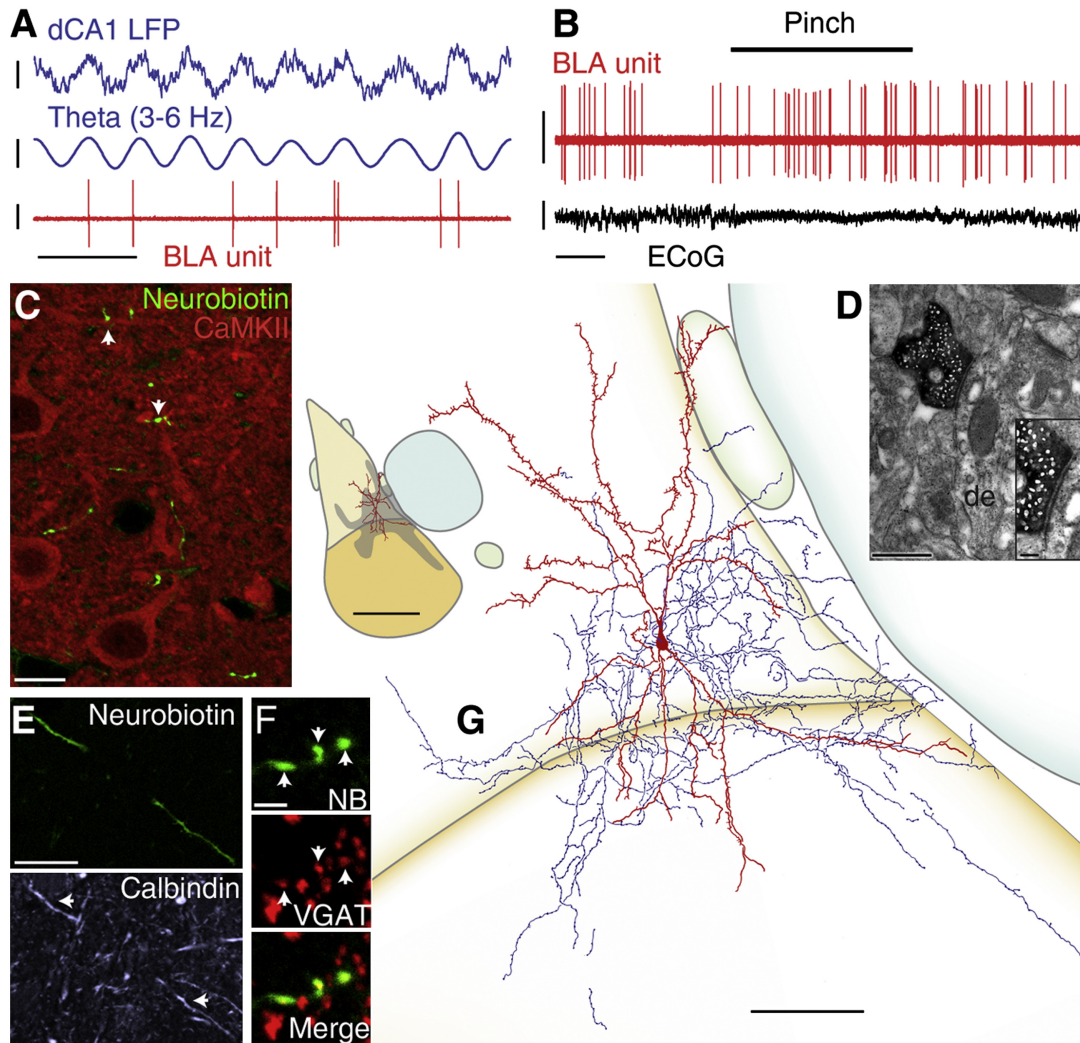


Figure 3. CB⁺ Dendrite-Targeting Cells: Firing In Vivo and Anatomical Characterization

(A) tjsx22c fired preferentially before the peak of dCA1 θ .

(B) tjsx59b did not change its firing rate during a noxious stimulus.

(C) Axon varicosities of tjsx21i avoid CaMKII⁺ somata and occasionally make visible appositions with CaMKII⁺ dendrites (arrows; projection of a confocal z stack of 2.10 μm thickness).

(D) Electron micrograph of a synapse formed by an axon bouton of tjsx22c with a CaMKII α ⁺ dendrite (de). Inset: higher magnification.

(E) tjsx22c is immunopositive for calbindin (structured illumination, single optical section).

(F) tjsx22c is GABAergic: confocal images (projection of z stack of 0.75 μm thickness) showing Neurobiotin (NB)-filled axon varicosities containing VGAT (arrows).

(G) Reconstruction of tjsx22c. Soma and entire dendritic tree are drawn from 8 sections of 60 μm thickness. Axon is drawn from 2 sections, for clarity. Inset: position of tjsx22c dendrites in the BLA and axonal field extent estimated from the two drawn and surrounding sections (color code as in Figure 1G). Orientation: top: dorsal, right: medial.

Scale bars: (A) LFP raw and filtered: 0.4 mV, unit: 1 mV, time: 400 ms; (B) unit: 1 mV, ECoG: 0.5 mV; (C) 10 μm ; (D) 500 nm, inset 100 nm; (E) 20 μm ; (F) 2 μm ; (G) 100 μm , inset 500 μm . See also Figures S1–S6 and Tables S1–S3.

CaMKII α (Figures 4D, 4E, and S6D). Most of the axons were distributed in the BLA, where they made dense ramifications (Figures 4C and S7B). Studied with light microscopy, a proportion of the large axon varicosities made multiple perisomatic contacts with CaMKII α ⁺ BLA principal neurons; the others possibly contacted small dendrites (Figure 4G). Electron microscopic analysis confirmed that postsynaptic targets in the lateral nucleus were dendrites (Figure 4F) and somata (35% and 65%,

respectively, $n = 40$ synapses, 2 cells; Table S1). Of these, 35% were confirmed CaMKII α ⁺ neurons (Figure 4F, Table S1). Dendrites targeted by AStria-projecting neurons were smaller than those postsynaptic to PV⁺ basket cells but larger than those targeted by CB⁺ dendrite-targeting cells (diameter $0.79 \pm 0.06 \mu\text{m}$, $p < 0.05$; Figure S6E).

All AStria-projecting neurons expressed PV (Figure 4H), and half also expressed CB. GABA α R- $\alpha 1$ was moderately enriched

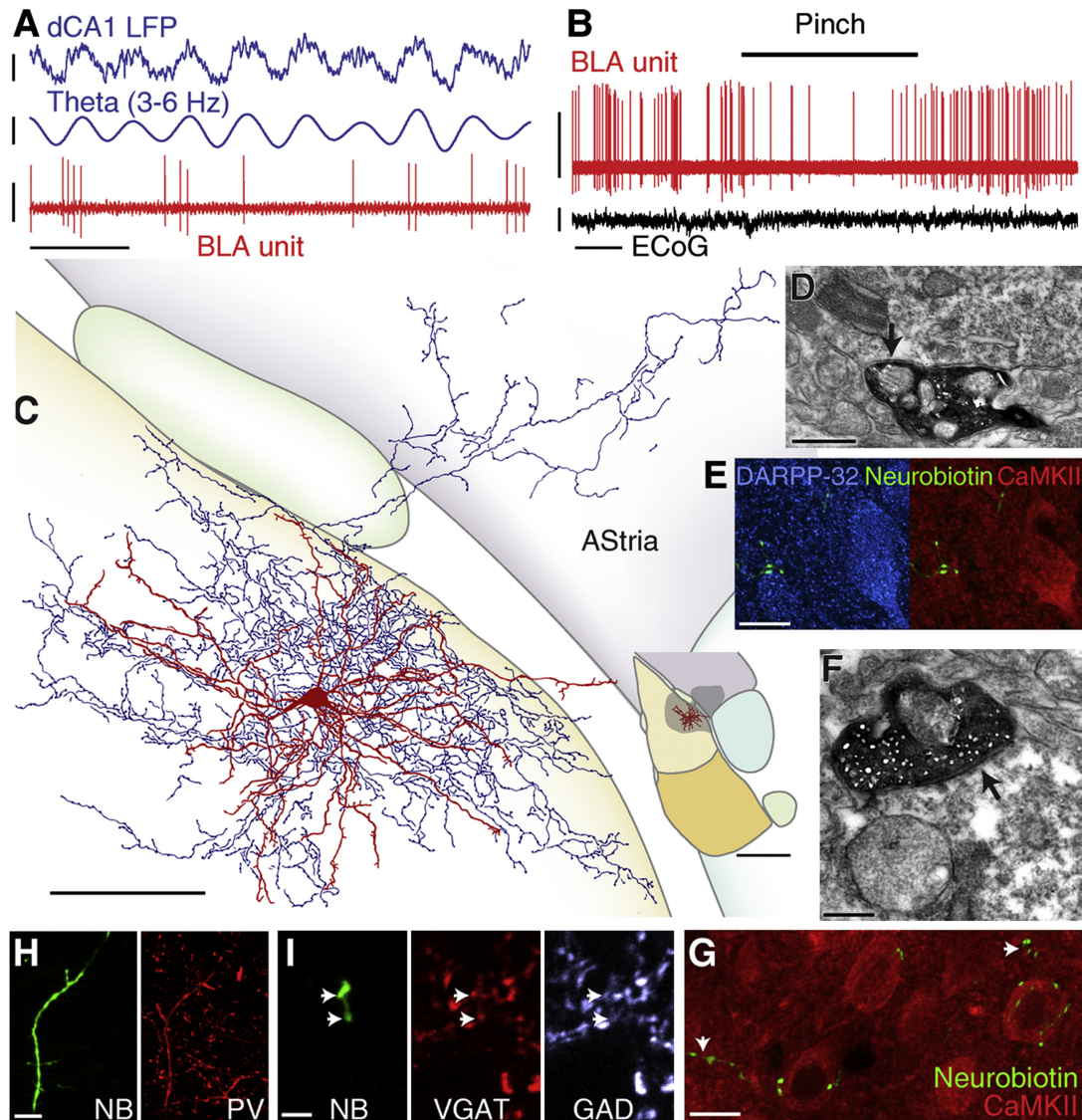


Figure 4. AStria-Projecting Cells: Firing In Vivo and Anatomical Characterization

All panels show data from one neuron (tjx52a).

(A) Preferential firing during the ascending phase of hippocampal θ oscillations.

(B) Reduced firing during hindpaw pinches.

(C) Reconstruction of tjx52a. Soma and entire dendritic tree are drawn from 5 sections of 60 μm thickness. Axon is drawn from 2 sections, for clarity. Inset: position of tjx52a dendrites in the BLA and axonal field extent in the two drawn and surrounding sections. Color code is as in Figure 1G, and AStria is purple. Orientation: top: dorsal, right: medial.

(D) Electron micrograph of a labeled bouton making a synapse (arrow) with a $\text{CaMKII}\alpha^+$ soma in the AStria.

(E) Axon varicosities making close appositions with a principal neuron ($\text{CaMKII}\alpha^+/\text{DARPP-32}^+$) soma in the AStria. Projection of a confocal z stack of 3.06 μm thickness.

(F) Electron micrograph of a labeled bouton making a synapse (arrow) with a $\text{CaMKII}\alpha^+$ principal cell dendrite in the lateral amygdala.

(G) Axon varicosities making close appositions with principal neuron somata ($\text{CaMKII}\alpha^+$) or unidentified structures (arrows) in the lateral amygdala (projection of confocal z stacks of 8.05 μm thickness).

(H) Immunopositivity for parvalbumin (structured illumination z stack; NB: Neurobiotin).

(I) tjx52a is GABAergic: confocal images (projections of z stack of 0.94 μm thickness) showing axon varicosities (arrows) positive for VGAT and GAD. NB: Neurobiotin.

Scale bars: (A) units and LFPs: 0.5 mV, time: 400 ms; (B) units 1 mV, time: 4 s; (C) 100 μm , inset 500 μm ; (D) 500 nm; (E) 10 μm ; (F) 250 nm; (G) 10 μm ; (H) 10 μm ; (I) Scale bar: 2.5 μm . See also Figures S1–S7 and Tables S1–S3.

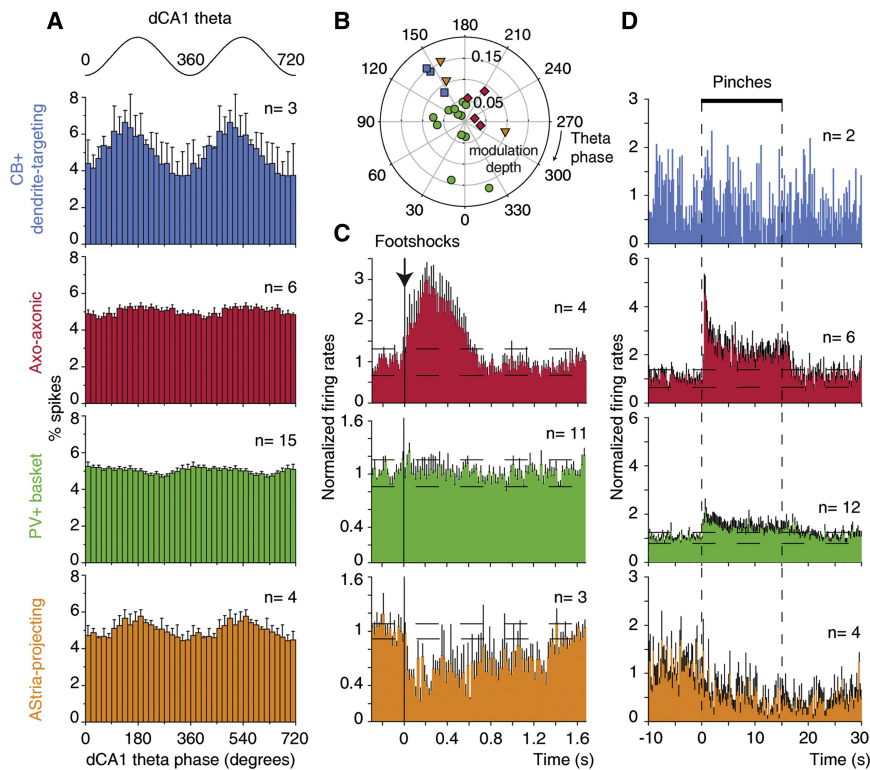


Figure 5. Firing Modulation with Hippocampal Theta Oscillations and Responses to Noxious Stimuli Are Cell Type Specific

(A) Cell types mean θ phase histograms. CB⁺ dendrite-targeting interneurons are homogeneously and strongly modulated in phase with dCA1 θ , in contrast to the other cell types. Two θ cycles are represented for clarity. 0°, 360°, and 720°: θ troughs.

(B) Polar distribution of individual neurons' preferred θ phases and modulation depths. Each symbol represents a significantly modulated cell. (C and D) Cell types mean peristimulus histograms for noxious stimulation. Axo-axonic cells are dramatically excited and AStria-projecting cells are inhibited by electrical shocks and pinches delivered to the contralateral hindpaw. Error bars: SEM; dashed lines: mean \pm 2 standard deviations. n values represent the number of neurons tested in each analysis.

See also Figures S2, S4, and S5.

in the plasma membrane of one cell but was never strongly expressed, in contrast to PV⁺ basket cells (Table S2). Dendrites were multipolar and branched profusely. They were short, smooth, and very tortuous (Figures 4C and S7B).

The distinct dendritic and axonal patterns and postsynaptic targets demonstrate that AStria-projecting cells may constitute a specific cell type. The present data indicate that they do not form a synchronous cell population with respect to dCA1 θ but dramatically decrease their firing in response to noxious stimuli (Figure 5).

Overall, various BLA interneuron types appear to fire differently in relation to network activities. However, they could not be separated on the basis of their spike shapes and durations (Figure S8; Table S5).

BLA Principal Neurons Fire Heterogeneously in Relation to Hippocampal Theta Oscillations

Next, we assessed the firing modulation of glutamatergic principal neurons in phase with hippocampal θ , because they are a major target of the interneurons defined above and represent the main output of the BLA ($n = 23$ cells; see Figure S1B for somata locations). Principal cells fired at very low rates during hippocampal θ (mean 0.29 Hz, range: 0.03–1.34 Hz; $n = 23$; Table S4). Irregular burst firing (2–3 spikes) was often observed, as reflected in high coefficients of variation of firing (CVs, which quantify irregularity of spike trains, 1.95 ± 0.13). Noteworthy, we found that principal cells fired longer-lasting spikes than all four types of interneurons (Figure S8; Table S5). Unsupervised cluster analysis could differentiate principal cells and interneurons (Figure S8C).

(Figure 6B). They coexpressed CaMKII α ($n = 14/14$ tested; Figure 6C; Table S4). Of the remaining eight neurons, three were weakly Neurobiotin-filled cells expressing CaMKII α , whereas the other five were unlabeled (see Supplemental Experimental Procedures).

The firing of 39% (9/23) of principal neurons was strongly modulated in phase with dCA1 θ oscillations (mean $r = 0.17$; Figure 6D; Table S4). The majority of BLA principal neurons thus fired independently of dCA1 θ . Theta-modulated cells did not form a tightly synchronized group ($R' = 0.72$, $R_{0.05,9} = 1.053$, Moore test; Figure 6D), in line with the weak ensemble (LFP) θ activity observed in the BLA. Importantly, the proportion of θ -modulated neurons and the preferred phase distribution (Figure 6E) were both consistent with previous studies in nonanesthetized animals (Paré and Gaudreau, 1996; Popa et al., 2010).

Modulation with Ventral Hippocampal Theta

The BLA receives dense innervation from the ventral hippocampal formation (McDonald, 1998; Pitkänen et al., 2000), but not from dCA1. However, dCA1 θ oscillations represent a more reliable reference signal compared with ventral hippocampal θ . In dCA1, the θ rhythm is regular, reproducible across animals and it has been suggested to indirectly but accurately reflect ventral hippocampal activities (Royer et al., 2010). Indeed, θ oscillations recorded from dorsal and ventral CA1 are coherent in both urethane-anesthetized and drug-free rats (Adhikari et al., 2010; Hartwich et al., 2009; Royer et al., 2010), and many ventral hippocampal neurons fire phase-locked to dCA1 θ (Hartwich et al., 2009; Royer et al., 2010). In contrast,

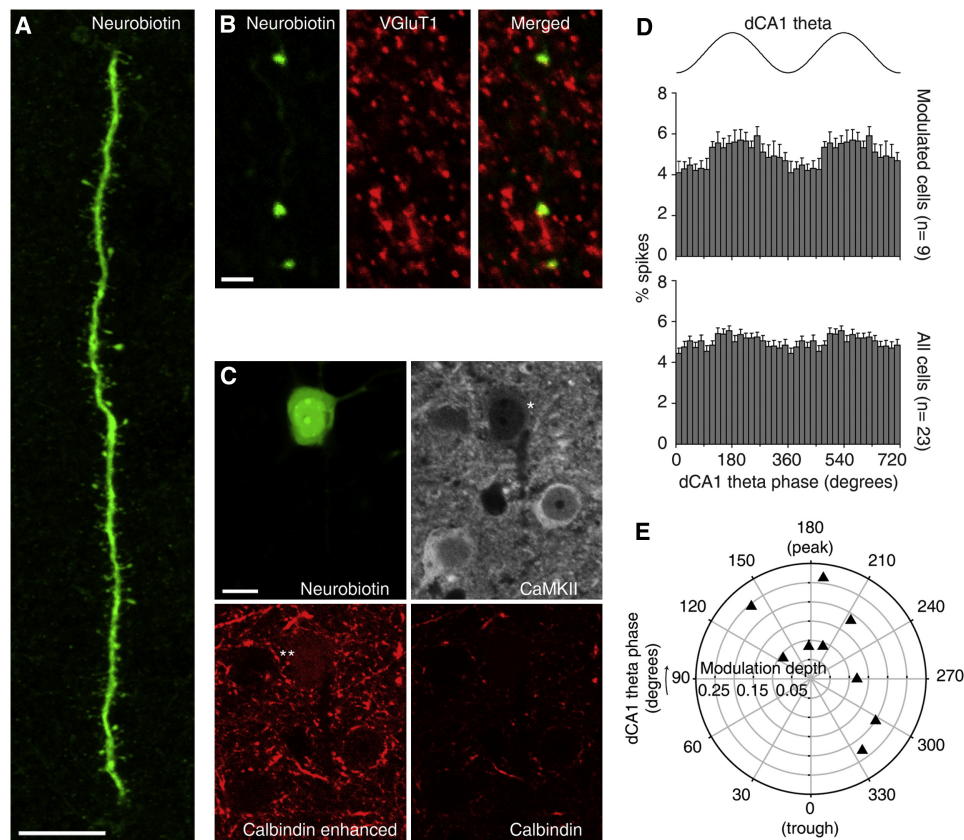


Figure 6. Anatomical Features and Theta Modulation of BLA Principal Neurons

(A) The neuron tjx89c had large dendrites covered with spines (projection of a confocal z stack of 7.99 μm thickness). (B) tjx89c expressed VGLUT1, demonstrating its identity as a glutamatergic neuron (single optical section confocal micrographs; recordings from this neuron are shown in Figure 7A). (C) Moderate levels of CaMKII α , (*) as well as weak calbindin (**) expression were detected in the soma of tjx89c (confocal images, single optical sections). (D) Phase histograms. Two θ cycles are shown for clarity. Error bars represent SEM. (E) Polar distribution of preferred θ phase and modulation depth of the θ -modulated principal neurons ($n = 9/23$). Each symbol represents a modulated neuron. Note that all 9 cells were strongly modulated. Scale bars (A) 10 μm ; (B) 2 μm (C) 10 μm . See also Figures S1 and S8, and Table S4.

LFP θ in ventral hippocampus would have been an unsuitable reference. LFP θ phase in ventral hippocampus varies dramatically between recordings, preventing a reliable comparison of phase locking between animals (Hartwich et al., 2009; Table S6). Moreover, ventral hippocampal θ oscillations have low amplitude and occur only transiently (Adhikari et al., 2010; Hartwich et al., 2009; Royer et al., 2010), compromising the isolation of θ epochs using unbiased methods (Csicsvari et al., 1999; Klausberger et al., 2003) and the calculation of θ phases.

To validate that dCA1 signal predicted spike timing of BLA neurons relative to ventral hippocampal θ , we performed experiments that included a vCA1-subiculum electrode ($n = 3$ animals, 6 neurons). Ventral stratum radiatum LFP signal was used as second reference. Theta oscillations were intermittent and had generally low amplitude, as reported in behaving rodents (Figure S9; Adhikari et al., 2010; Royer et al., 2010).

As expected, dCA1 signal predicted BLA unit firing modulation with ventral hippocampal θ . Differences between the phases of dCA1 and vCA1-subiculum LFP θ oscillations were similar to,

and correlated with the difference between the preferred phases of neuron firing calculated with the two references (Pearson's correlation $r = 0.975$, $p = 0.025$ and circular-circular correlation: Fisher and Lee's method, Oriana software, $p < 0.05$, $n = 4$: 3 principal cells, 1 PV+ basket cell; Figures 7 and S9). Moreover, θ modulation strengths of units calculated with dorsal and ventral hippocampal references were similar and linearly correlated (Pearson's correlation $r = 0.976$, $p = 0.024$; $n = 4$; Figure 7D). These results establish that dCA1 is a suitable and sensitive reference to study the coupling of BLA neuron firing to hippocampal θ .

DISCUSSION

This study defines several types of BLA interneurons and their role in shaping BLA activity in relation to dCA1 θ oscillations and noxious stimuli, two processes critical in forming emotional memories. The key findings are the following: dendrite-targeting CB⁺ interneurons provide inhibition to BLA principal cells in

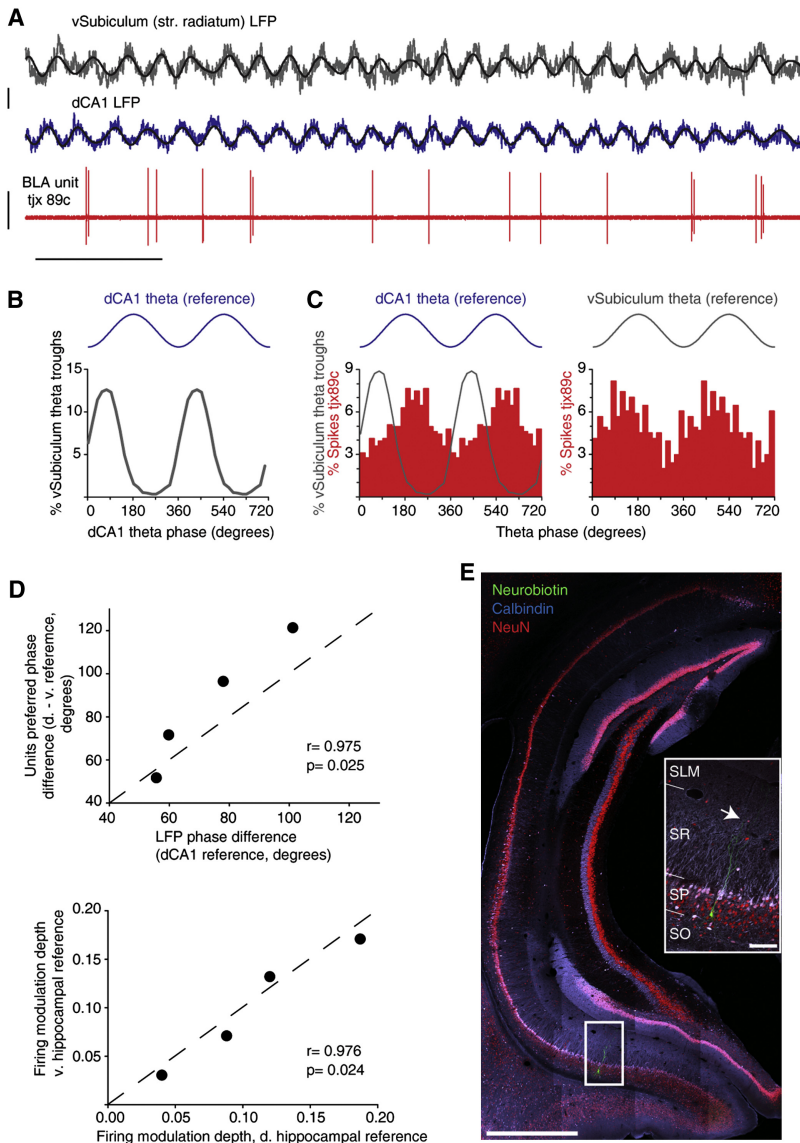


Figure 7. Dorsal CA1 Reference Recapitulates BLA Unit Firing Modulation by Ventral Hippocampal θ

(A and B) A principal neuron (tjr89c) was recorded along with LFPs from dorsal (CA1 str. pyramidale) and vHippocampus (subiculum str. radiatum). (A) Raw data showing tjr89c firing during an exemplary period of ventral hippocampal θ . Traces filtered for θ frequencies are overlaid. (B) Theta oscillations in the ventral subiculum are phase-locked to those in dCA1. Phase histogram representing the distribution of vSubiculum θ troughs across the dCA1 θ cycle.

(C and D) Single units modulated in phase with dCA1 θ are similarly modulated with vHippocampus θ . (C) Left: phase histogram of tjr89c spikes computed with the dCA1 reference. vSubiculum θ trough distribution was superimposed to illustrate the predicted firing phase relationship of tjr89c with vSubiculum θ rhythm (predicted phase: 135.7°). Right: distribution of tjr89c spike angles relative to vSubiculum θ , consistent with the prediction. (D) Results obtained with dCA1 θ phase as a reference accurately reflect firing modulation of neurons in phase with ventral hippocampal θ . Top: linear correlation between the predicted (LFPs) and actual phase differences of neuron modulation by dorsal and ventral hippocampal θ . Bottom: linear correlation between modulation depths calculated with the dorsal and ventral hippocampal references. Diagonal dashed lines: unity line.

(E) Anatomically confirmed recording sites in the ventral subiculum from the same experiment. The white box highlights the Neurobiotin (green) deposit made at the str. pyramidale recording site. NeuN immunoreactivity (red) was used as a panneuronal nuclear and cytoplasmic marker to delineate str. pyramidale. Calbindin immunoreactivity (light blue) highlights hippocampal layers. Colocalization with NeuN is indicated by white and pink. Inset: higher magnification of the area delineated in the main panel. Arrow: recording site in str. radiatum. SO: str. oriens; SP: str. pyramidale; SR, str. radiatum; SLM: str. lacunosum moleculare.
Scale bars: (A) time: 1 s, LFPs: 0.5 mV, units: 2 mV; (E) 1 mm, inset: 100 μ m. See also Figure S9 and Table S6.

phase with hippocampal θ oscillations. The firing of PV⁺ basket cells is not tightly synchronized with θ oscillations. Axo-axonic cells consistently and dramatically increase their firing in response to noxious stimuli. In addition, we discovered a GABAergic cell type well placed to coordinate spontaneous and sensory-related BLA-Astria interactions. Our results support the hypothesis that interneurons are critical in regulating timing in the BLA, and that they operate in a cell-type-specific manner. We demonstrate that this principle is not limited to firing relationships with ongoing oscillations, but also applies to the integration of sensory information.

GABAergic Cell Types of the BLA

Defining cell types requires the correlated analysis of molecular markers, full dendritic and axonal patterns and postsynaptic targets at ultrastructural level (Somogyi, 2010). The present study unambiguously defines four interneuron types of the BLA.

First, we demonstrate that axo-axonic and PV⁺ basket cells are two distinct cell types in the rat BLA. Indeed, PV⁺ basket cells target somata and dendrites of principal neurons, whereas axo-axonic cells innervate almost exclusively axon initial segments. Thus, the hypothesis that axo-axonic and PV⁺ basket cells of BLA are a single cell type (Woodruff et al., 2006) should be rejected, at least in adult rats. The present report of an extensive coexpression of PV, CB, and/or GABA_A- α 1 in BLA interneurons is consistent with earlier studies (McDonald and Betette, 2001; McDonald and Mascagni, 2004). Our data suggest that the coexpression of moderate to high levels of PV, CB, and GABA_A- α 1 may be specific to basket cells.

Second, we identified a CB⁺ dendrite-targeting cell type. The existence in the BLA of such PV⁺ interneurons specifically targeting dendrites has been inferred (Muller et al., 2006; Woodruff et al., 2006; Woodruff and Sah, 2007), but never directly demonstrated. The target selectivity of basket and dendrite-targeting

cells demonstrates a clear separation, and precludes their grouping into a single population.

Third, we report a specific GABAergic cell type, that we named AStria-projecting, for its axon reaching outside the BLA.

The BLA most likely comprises additional GABAergic cell types (Ehrlich et al., 2009). Indeed, Golgi staining has revealed BLA interneurons with axo-dendritic patterns distinct from those presented here (e.g., neurogliaform-like cells, McDonald, 1982). Moreover, populations of BLA GABAergic neurons lacking PV have been shown to express markers such as calretinin, cholecystokinin, neuropeptide Y, or somatostatin (Spampanato et al., 2011). Recent *in vitro* studies have elucidated the firing characteristics, dendritic and axonal patterns, expression of neurochemical markers, and functional connectivity of some of these neurons (Jasnow et al., 2009; Rainnie et al., 2006; Sosulina et al., 2010). However, the lack of a comprehensive anatomical strategy has so far prevented a clear characterization of these interneuron types.

We demonstrated that different BLA interneuron types make GABAergic synapses with specific domains of principal cells. This appears of key significance in light of their distinct firing activities.

Firing Relationship with Hippocampal Oscillations

The firing relation of BLA interneurons to hippocampal θ differed between cell types. This is consistent with only a subset of putative BLA interneurons firing in phase with hippocampal θ in behaving cats (Paré and Gaudreau, 1996). Importantly, the modulation strength of interneuron activity was independent from the power and frequency of dCA1 θ oscillations (Experimental Procedures).

Dendrite-targeting CB⁺ cells showed the most consistent firing modulation. The dendritic inhibition they provide could modulate the integration of glutamatergic inputs and limit action potential back-propagation, thereby rendering synaptic plasticity onto principal neurons dependent on hippocampal θ . This is particularly important in the BLA, where synaptic plasticity on dendritic spines is thought to underlie fear memory encoding (Humeau et al., 2005; Ostroff et al., 2010).

We found weak and inconsistent θ -modulation of PV⁺ basket and axo-axonic cell firing, which both innervate the perisomatic domain of target cells. At the population level, these cells appear to provide constant perisomatic inhibition of principal neurons. We cannot rule out that synchronization is limited to subpopulations of these neurons. Somata of BLA principal cells are innervated by ~60 PV⁺ boutons and their axon initial segment by ~20 boutons (Muller et al., 2006). Terminals of PV⁺ fast-spiking cells release GABA with high fidelity (Hefft and Jonas, 2005). Together with our results, this suggests that ~900 boutons release GABA around each BLA principal cell soma every second. Such powerful inhibition likely contributes to the very low firing rates of principal neurons, provided axo-axonic cells chiefly inhibit postsynaptic cells (Woodruff et al., 2011). Our finding of weakly θ -related activity of perisomatic-innervating cells constitutes a major difference from what has been reported in neocortex and hippocampus (Hartwich et al., 2009; Klausberger et al., 2003). Individual AStria-projecting cells might provide θ -modulated perisomatic inhibition to their target

neurons in BLA and AStria, but they do not seem to play such a role as a population.

Interneurons might adjust their relationship with θ rhythms on a fine time-scale, possibly depending on behavioral states. The present analysis assumes relatively stationary activities and was not designed to capture specific bouts of dynamic synchronization. The juxtacellular method used here restricts sample sizes. It is possible that large assemblies of interneurons whose activity is weakly synchronized can still have a large net effect on principal neuron populations.

None of the recorded interneurons showed modulation in phase with dCA1 γ oscillations. This held true for the analysis of θ -nested γ oscillations and for entire γ oscillation periods. Our findings are consistent with γ oscillations being generated locally and indicate that BLA interneurons are more likely to participate in amygdalo-hippocampal synchrony at θ frequencies.

The firing of ~40% of principal cells was strongly modulated in phase with hippocampal θ . Modulated cells could correspond to the so-called fear neurons, which selectively receive inputs from ventral hippocampus (Herry et al., 2008). As found in behaving rats, preferred θ phases of principal cells were dispersed (Popa et al., 2010). Phase-modulation heterogeneity may result from the convergence at heterogeneous phases of perisomatic inhibition (as our data suggest) and of excitatory inputs from several brain regions. For example, perirhinal and entorhinal cortices also innervate the BLA (McDonald, 1998; Pitkänen et al., 2000) and contain neuronal assemblies oscillating at θ frequencies (Collins et al., 1999).

Firing Responses to Noxious Stimuli

Salient sensory events recruit the amygdala to attach emotional significance to coincident neutral stimuli (LeDoux, 2000). Previous work suggests that phasic GABAergic inhibition may be instrumental in integrating noxious stimuli, by increasing synchrony in the BLA (Crane et al., 2009; Windels et al., 2010). Diversity in roles played by interneuron types could be expected not only during spontaneous activity, but also in integrating salient sensory stimuli. Indeed, we found cell-type-dependent responses to noxious stimuli.

AStria-projecting neurons responded with a long-lasting inhibition of firing. Their target neurons in amygdala and AStria should be concomitantly disinhibited, perhaps promoting Hebbian synaptic plasticity. While the functions of AStria neurons are unknown, they might be involved in appetitive behavior and potentially participate in a parallel circuit controlling emotional responses.

In contrast, the firing of axo-axonic cells increased systematically and dramatically upon noxious stimuli presentation. Inputs from extrinsic afferents might mediate this effect. The responses of axo-axonic cells to noxious events may trigger the stimulus-induced GABAergic currents recorded in principal cells, thus generating synchrony in the BLA (Windels et al., 2010). Axo-axonic cells could provide temporal precision to large principal cell assemblies for the encoding of associations with unconditioned stimuli, in two ways: (1) by synchronizing principal neurons for glutamatergic inputs subsequently reaching the BLA; (2) by limiting the synaptic integration time window (Pouille and

Scanziani, 2001), thus controlling spike-timing-dependent plasticity (Humeau et al., 2005). Activation of GABA_B receptors, specifically expressed on glutamatergic inputs to BLA principal neurons (Pan et al., 2009), might also reinforce the temporal precision of synaptic plasticity (Humeau et al., 2003). Alternatively, the response of axo-axonic cells might restrict principal cell firing to those most strongly excited by noxious stimuli.

The stimuli used in this study closely resemble those employed in classical fear conditioning experiments. Therefore, our results predict how BLA interneurons might be involved in fear learning. The present results were obtained from urethane-anesthetized rats. We cannot rule out that firing patterns of BLA neurons are different in behaving animals. However, reports on responses of single units to visual or auditory cues in different brain regions and species have found strong similarities between awake and urethane anesthesia states (Niell and Stryker, 2010; Schumacher et al., 2011). Spontaneous firing frequencies appear decreased by urethane, whereas direction and magnitude of sensory-evoked responses seem unaffected. Urethane treatment induces brain states comparable to those observed in natural conditions (Clement et al., 2008). Hippocampal θ oscillations display patterns resembling those in the unanaesthetized state (Lubenov and Siapas, 2009, and our results). In addition, we found that BLA principal neurons fired similarly phase-locked to hippocampal θ as previously reported in behaving animals. In hippocampus, groups of putative interneurons recorded in behaving rats appear similarly θ -modulated to the main GABAergic cell classes recorded under urethane (Czurkó et al., 2011). Overall, it is likely that firing patterns of BLA neurons reported here recapitulate their main characteristics in drug-free conditions.

BLA Theta Genesis

BLA-hippocampal theta synchronization increases after fear conditioning. This might facilitate the cortical transfer of emotional memories for long term storage (Paré et al., 2002; Popa et al., 2010). How may specific firings of GABAergic interneurons contribute to this? Convergent excitatory inputs onto principal cells during sensory stimuli can trigger synaptic plasticity (Humeau et al., 2003). Dendrite-targeting interneurons, such as those CB⁺ cells, could provide powerful inhibitory control of such excitatory inputs (Lovett-Barron et al., 2012). Calbindin⁺ interneurons preferentially fire before the peak of dCA1 θ . Therefore, excitatory inputs active around the θ trough are more likely to increase their synaptic weight during intense sensory stimulation.

Axo-axonic cells may ensure that synaptic potentiation is restricted to inputs concomitantly active with the salient stimulus. Assuming that some extrinsic inputs are θ -modulated, the net effect could be a stronger θ modulation of excitatory input to BLA principal neurons. This potentiation would create synchrony in large cell assemblies in synergy with the intrinsic membrane potential resonance of BLA principal neurons (Paré et al., 1995). Consistent with this, LFP θ power increases in BLA following fear conditioning (Paré and Collins, 2000; Seidenbecher et al., 2003), and BLA principal neurons become more θ modulated and synchronous after fear conditioning (Paré and Collins, 2000). These changes are made possible by the fact

that in naive animals, only 20%–40% (Popa et al., 2010, and our findings) of BLA principal neurons are θ -modulated, and at dispersed phases. BLA θ oscillations increase after fear conditioning with a delay (Pape et al., 2005; Paré et al., 2002), which may be explained by the induction of structural plasticity (Ostroff et al., 2010).

The present results suggest that PV⁺ basket and axo-axonic cells play minor roles in θ increase. However, they might modify their activities with emotional learning and later support BLA θ oscillations. Futures work in behaving animals is needed to examine the activities of BLA interneurons after fear conditioning and, most critically, to address how they change during learning. Our finding of cell-type-dependent firing could be used to facilitate the classification of putative BLA interneurons recorded in behaving animals.

Conclusion

Modulation of neuronal synchrony in the BLA is critical for the formation of emotional memories. This study provides insights into the cell type-specific contribution of GABAergic cells to BLA synchrony. Timed release of GABA on specific domains of BLA principal neuron is likely important for emotional information processing. We propose that the cooperation between precise spike-timing of various interneuron types is necessary for the encoding and persistence of emotional memories. Future studies could build on our findings to manipulate specific interneuron populations during behavior and directly test this hypothesis.

EXPERIMENTAL PROCEDURES

In Vivo Electrophysiological Recordings

All procedures involving experimental animals were performed in accordance with the Animals (Scientific Procedures) Act, 1986 (UK) and associated regulations, under approved project and personal licenses. Seventy adult male Sprague-Dawley rats (250–350 g) were anesthetized with intraperitoneal injections of urethane (1.30 g.kg⁻¹ body weight) plus supplemental doses of ketamine and xylazine, (10–15 and 1–1.5 mg.kg⁻¹, respectively) as needed. The rectal temperature was maintained at 37°C with a homeothermic heating device. Craniotomies-duratomies were performed over the right hippocampus and amygdala.

Neuronal activities in the BLA and dCA1 (stratum oriens-pyramidale) were recorded with independent electrodes made of silver-chloride wires loaded in glass pipettes filled with 1.5% Neurobiotin (Vector Laboratories) in 0.5 M NaCl (12–18 M Ω resistance in vivo, tip diameter \sim 1.1 μ m). Glass electrode signals were referenced against a wire implanted subcutaneously in the neck. The electrocorticogram (ECoG) was recorded via a 1 mm diameter steel screw juxtaposed to the dura mater above the right prefrontal cortex (Bregma AP: 4.5 mm, ML: 2.0 mm), and was referenced against a screw implanted above the ipsilateral cerebellum.

Pinches of 15 s duration were delivered to the hindpaw contralateral to recording sites using pneumatically driven forceps that delivered a pressure of 183 g.mm⁻². Similar mechanical stimuli have been shown to be noxious by eliciting an escape response in behaving rats, as well as by recruiting nociceptive brain circuits in urethane-anesthetized rats (Cahusac et al., 1990). Electrical stimuli (single current pulses of 5 mA intensity and 2 ms duration) were delivered at 0.5 Hz through 2 wires implanted on the ventral face of the contralateral hindpaw, for at least 100 trials. The timing of stimuli delivery was controlled by an external pulse generator (Master-8; A.M.P.I.) and synchronously recorded. Identical electrical shocks have been shown to activate spinal cord nociceptive neurons in urethane-anesthetized rats (Coizet et al., 2006).

Residual 50 Hz noise and its harmonics were reduced in all signals using Humbugs (Quest Scientific). Glass electrode signals were amplified (10×, Axoprobe 1A, Molecular Devices Inc.), bifurcated, further amplified (100×), and differentially filtered (DPA-2FS filter/amplifier; Scientifica) to extract local field potentials (LFPs, 0.3–5,000 Hz) and unit activities (300–5,000 Hz). Raw ECoG signal was band-pass filtered (0.3–1,500 Hz) and amplified (2,000×). All signals were digitized online at 16.67 kHz using a Power 1401 analog-digital converter (Cambridge Electronic Design) and stored on a PC running Spike2 software (versions 6.08 and 6.09, Cambridge Electronic Design). GABAergic cell recordings lasted 15–105 min (typically ~45 min). The juxtacellular recording mode (rather than, for example, a quasi-intracellular mode), was assured by only including for analysis neurons that (1) had stable spontaneous firing rates/patterns and stable spike widths; (2) did not display any “injury discharge”; and (3) were recorded in the absence of spurious “baseline noise” or hyperpolarizing shifts in the electrode potential.

Labeling of Single Neurons and Reference Sites

After recordings, neurons were selectively filled with Neurobiotin using juxtacellular labeling (Pinault, 1996). Spike shape and amplitude were monitored throughout recording and labeling to ensure that the same neuron was recorded and labeled. In order to verify the location of the reference electrode, an extracellular Neurobiotin deposit was made in the dorsal CA1 (100 nA anodal current 1 s, 50% duty cycle for 20–30 min).

Electrophysiological Data Analysis

Only data acquired before labeling and obtained from unequivocally identified cells were analyzed. All data were analyzed off-line using Spike2 built-in functions and custom scripts (Tukker et al., 2007). Spikes were detected with an amplitude threshold in the BLA unit channel. Occasionally, additional smaller amplitude units were present in the recording. Spike2 clustering function supervised manually was used to isolate single units, and identity of labeled neurons was systematically ensured as described above. Spike sorting was always checked using autocorrelograms, which showed clear refractory periods (≥ 2 ms).

Hippocampal theta oscillation epochs were detected by calculating the theta (3–6 Hz) to delta (2–3 Hz) power ratio in 2 s windows of the dCA1 LFP (Csicsvari et al., 1999; Klausberger et al., 2003). Ratio >4 in at least three consecutive windows marked theta episodes. We excluded from this analysis periods of noxious stimuli and the following 20 s. Every theta episode was visually checked. Selected periods always consisted of robust theta oscillations. They exclusively occurred during persistently activated brain state (Figure S9). After theta episodes detection, the dCA1 LFP was downsampled to 1.04 kHz, digitally filtered (3–6 Hz) and the troughs were determined (Spike2). Each spike was assigned an angle relative to surrounding theta troughs (Tukker et al., 2007; Klausberger et al., 2003). The precision of our electrode placements (mediolateral and antero-posterior ranges ~ 400 μm) ensured phase consistency between experiments (i.e., ~ 8.5 degrees error, assuming a phase shift of $21^\circ/\text{mm}$; Lubenov and Siapas, 2009).

Mean firing frequency was calculated over 100 s continuous periods of robust theta activity. Coefficient of variation (S.D./mean, CV) of interspike intervals during these periods was used as a measure of firing regularity. CV greater than 1 indicated the cell fired in an irregular pattern.

Responses to noxious stimuli were assessed by constructing peristimulus histograms (bin size 20 ms for electrical footshocks, 200 ms for hindpaw pinches). Responses were analyzed only if the brain state corresponded to stable global activation before, during, and after the noxious stimulus. This allowed for the distinction of sensory-driven responses from effects on the brain state (e.g., change from slow wave to activation). In addition, we verified that hindpaw pinches did not induce changes in the power of the LFP oscillations recorded in dCA1 or BLA (θ and γ bands; $p > 0.05$, Wilcoxon signed-rank test, $n = 25$ cells).

Statistical Testing

Relation to hippocampal theta oscillations: all 833–20,522 (average 6,906) spike angle values from single interneuron units were exported for testing with circular statistics (Oriana v. 2.0, Kovac Computing Services). Modulation in phase with dCA1 theta oscillations was tested for significance using

Rayleigh's uniformity test (significance $p < 0.005$). If $p < 0.005$, the sum vector of all spikes was computed and normalized by the number of spikes. Its orientation determined the mean angle of spike firing, with respect to the trough (0°) of dCA1 theta oscillation (180° represents the theta peak). The length r of the normalized vector determined modulation depth. Phase modulation homogeneity within neuron groups (only modulated cells included) was tested with Moore's non parametric test (Zar, 1999). The null hypothesis was the absence of directionality in the group. If $p < 0.05$, cells of the group fired at consistent phases and Batschelet's method was used to calculate the population mean angle (Zar, 1999). This ensured the statistical reliability of our conclusions on population modulation. Furthermore, we established that the depth of modulation of BLA interneurons activity was not correlated with either the power or the mean frequency of dCA1 theta oscillations (Pearson correlation, $R = 0.03$, $p = 0.896$; $R = 0.216$, $p = 0.335$; respectively, $n = 22$).

Significance of responses to noxious stimuli was tested using thresholds. Footshocks: significance was accepted if at least 3 consecutive bins differed from the preonset 300 ms mean by 2 SD or any bin by 4 SD. Pinches: for 1–2 trials, significance was accepted if at least 3 consecutive bins differed from the preonset 10 s mean by 1 SD or any 1 bin by 4 SD. For 3 trials and more, significance was accepted if at least 3 consecutive bins differed from the preonset mean by 1.5 SD or any 1 bin by 4 SD. Latency was defined as the starting time of the first bin meeting these criteria. The peak time was the starting time of the largest change in the first significant series.

Differences in postsynaptic dendrite diameter between cell subgroups were evaluated using the Kruskal-Wallis test followed by Dunn's post hoc analysis.

Data are expressed as mean \pm SEM, unless otherwise stated.

Tissue Processing and Anatomical Analysis

Details on brains fixation, immunofluorescence, electron microscopy, and camera lucida reconstructions are given in the Supplemental Information.

SUPPLEMENTAL INFORMATION

Supplemental Information includes nine figures, eight tables, and Supplemental Experimental Procedures and can be found with this article online at doi:10.1016/j.neuron.2012.04.022.

ACKNOWLEDGMENTS

The authors thank R. Hauer, L. Norman, and K. Whitworth for excellent technical assistance. B.R. Micklem helped creating figures. J.-M. Fritschy and P. Greengard and A. Nairn kindly provided antibodies (anti-GABA_AR- $\alpha 1$ and anti-DARPP-32, respectively). Y. Dalezios, Linda Katona, and D. Lapray are acknowledged for their help with statistical analysis. We are most grateful to P. Somogyi for his guidance throughout the study, particularly on the collection and interpretation of anatomical data, and for his comments on the paper. We also thank C. Herry, M. Mańko, O. Paulsen, A. Sharott, and R. Stewart for critically commenting on earlier versions of the manuscript. This work was supported by the Medical Research Council, UK to M.C. (MRC award U138197106) and P.J.M. (MRC award U138197109), the Austrian Science Fund-Fonds zur Förderung der wissenschaftlichen Forschung (FWF) grant S10207 and W01206-10 to F.F. and by the Academic Research Collaboration Program of the British Council to F.F. and M.C. T.C.M.B. was funded by an MRC DPhil studentship, and is a fellow of Ecole de l'Inserm Liliane Bettencourt MD-PhD Program, France. All the authors participated in designing the study. Experiments were performed by T.C.M.B. (in vivo recordings, histological processing, neuron identification) and D.B. (electron microscopy, neuron reconstructions). P.J.M., F.F., and M.C. supervised the project. All the authors analyzed the data. T.C.M.B., P.J.M., F.F., and M.C. wrote the paper. All the authors commented on the paper and agreed on the final version of the manuscript.

Accepted: April 27, 2012

Published: June 20, 2012

REFERENCES

- Adhikari, A., Topiwala, M.A., and Gordon, J.A. (2010). Synchronized activity between the ventral hippocampus and the medial prefrontal cortex during anxiety. *Neuron* 65, 257–269.
- Anderson, K.D., and Reiner, A. (1991). Immunohistochemical localization of DARPP-32 in striatal projection neurons and striatal interneurons: implications for the localization of D1-like dopamine receptors on different types of striatal neurons. *Brain Res.* 568, 235–243.
- Bonifazi, P., Goldin, M., Picardo, M.A., Jorquera, I., Cattani, A., Bianconi, G., Represa, A., Ben-Ari, Y., and Cossart, R. (2009). GABAergic hub neurons orchestrate synchrony in developing hippocampal networks. *Science* 326, 1419–1424.
- Cahusac, P.M., Morris, R., Salt, T.E., and Hill, R.G. (1990). Sensory responses of caudal trigeminal neurons to thermal and mechanical stimuli and their behavioural correlates in the rat. *Neuroscience* 36, 543–551.
- Clement, E.A., Richard, A., Thwaites, M., Ailon, J., Peters, S., and Dickson, C.T. (2008). Cyclic and sleep-like spontaneous alternations of brain state under urethane anaesthesia. *PLoS One* 3, e2004.
- Cobb, S.R., Buhl, E.H., Halasy, K., Paulsen, O., and Somogyi, P. (1995). Synchronization of neuronal activity in hippocampus by individual GABAergic interneurons. *Nature* 378, 75–78.
- Coizet, V., Dommett, E.J., Redgrave, P., and Overton, P.G. (2006). Nociceptive responses of midbrain dopaminergic neurones are modulated by the superior colliculus in the rat. *Neuroscience* 139, 1479–1493.
- Collins, D.R., Lang, E.J., and Paré, D. (1999). Spontaneous activity of the perirhinal cortex in behaving cats. *Neuroscience* 89, 1025–1039.
- Crane, J.W., Windels, F., and Sah, P. (2009). Oscillations in the basolateral amygdala: aversive stimulation is state dependent and resets the oscillatory phase. *J. Neurophysiol.* 102, 1379–1387.
- Csicsvari, J., Hirase, H., Czurkó, A., Mamiya, A., and Buzsáki, G. (1999). Oscillatory coupling of hippocampal pyramidal cells and interneurons in the behaving Rat. *J. Neurosci.* 19, 274–287.
- Czurkó, A., Huxter, J., Li, Y., Hangya, B., and Muller, R.U. (2011). Theta phase classification of interneurons in the hippocampal formation of freely moving rats. *J. Neurosci.* 31, 2938–2947.
- Ehrlich, I., Humeau, Y., Grenier, F., Ciochchi, S., Herry, C., and Lüthi, A. (2009). Amygdala inhibitory circuits and the control of fear memory. *Neuron* 62, 757–771.
- Faber, E.S., Callister, R.J., and Sah, P. (2001). Morphological and electrophysiological properties of principal neurons in the rat lateral amygdala in vitro. *J. Neurophysiol.* 85, 714–723.
- Hartwich, K., Pollak, T., and Klausberger, T. (2009). Distinct firing patterns of identified basket and dendrite-targeting interneurons in the prefrontal cortex during hippocampal theta and local spindle oscillations. *J. Neurosci.* 29, 9563–9574.
- Hefft, S., and Jonas, P. (2005). Asynchronous GABA release generates long-lasting inhibition at a hippocampal interneuron-principal neuron synapse. *Nat. Neurosci.* 8, 1319–1328.
- Herry, C., Ciochchi, S., Senn, V., Demmou, L., Müller, C., and Lüthi, A. (2008). Switching on and off fear by distinct neuronal circuits. *Nature* 454, 600–606.
- Humeau, Y., Shaban, H., Bissière, S., and Lüthi, A. (2003). Presynaptic induction of heterosynaptic associative plasticity in the mammalian brain. *Nature* 426, 841–845.
- Humeau, Y., Herry, C., Kemp, N., Shaban, H., Fourcaudot, E., Bissière, S., and Lüthi, A. (2005). Dendritic spine heterogeneity determines afferent-specific Hebbian plasticity in the amygdala. *Neuron* 45, 119–131.
- Jasnow, A.M., Ressler, K.J., Hammack, S.E., Chhatwal, J.P., and Rainnie, D.G. (2009). Distinct subtypes of cholecystokinin (CCK)-containing interneurons of the basolateral amygdala identified using a CCK promoter-specific lentivirus. *J. Neurophysiol.* 101, 1494–1506.
- Jeon, D., Kim, S., Chetana, M., Jo, D., Ruley, H.E., Lin, S.Y., Rabah, D., Kinet, J.P., and Shin, H.S. (2010). Observational fear learning involves affective pain system and Cav1.2 Ca²⁺ channels in ACC. *Nat. Neurosci.* 13, 482–488.
- Klausberger, T., Magill, P.J., Márton, L.F., Roberts, J.D., Cobden, P.M., Buzsáki, G., and Somogyi, P. (2003). Brain-state- and cell-type-specific firing of hippocampal interneurons in vivo. *Nature* 421, 844–848.
- LeDoux, J.E. (2000). Emotion circuits in the brain. *Annu. Rev. Neurosci.* 23, 155–184.
- Lovett-Barron, M., Turi, G.F., Kaifosh, P., Lee, P.H., Bolze, F., Sun, X.H., Nicoud, J.F., Zemelman, B.V., Sternson, S.M., and Losonczy, A. (2012). Regulation of neuronal input transformations by tunable dendritic inhibition. *Nat. Neurosci.* 15, 423–430, S421–S423.
- Lubenov, E.V., and Siapas, A.G. (2009). Hippocampal theta oscillations are travelling waves. *Nature* 459, 534–539.
- Maren, S., and Fanselow, M.S. (1995). Synaptic plasticity in the basolateral amygdala induced by hippocampal formation stimulation in vivo. *J. Neurosci.* 15, 7548–7564.
- Mascagni, F., and McDonald, A.J. (2003). Immunohistochemical characterization of cholecystokinin containing neurons in the rat basolateral amygdala. *Brain Res.* 976, 171–184.
- McDonald, A.J. (1982). Neurons of the lateral and basolateral amygdaloid nuclei: a Golgi study in the rat. *J. Comp. Neurol.* 212, 293–312.
- McDonald, A.J. (1998). Cortical pathways of the mammalian amygdala. *Prog. Neurobiol.* 55, 257–332.
- McDonald, A.J., and Bette, R.L. (2001). Parvalbumin-containing neurons in the rat basolateral amygdala: morphology and co-localization of Calbindin-D(28k). *Neuroscience* 102, 413–425.
- McDonald, A.J., and Mascagni, F. (2004). Parvalbumin-containing interneurons in the basolateral amygdala express high levels of the alpha1 subunit of the GABA_A receptor. *J. Comp. Neurol.* 473, 137–146.
- Muller, J.F., Mascagni, F., and McDonald, A.J. (2006). Pyramidal cells of the rat basolateral amygdala: synaptology and innervation by parvalbumin-immunoreactive interneurons. *J. Comp. Neurol.* 494, 635–650.
- Niell, C.M., and Stryker, M.P. (2010). Modulation of visual responses by behavioral state in mouse visual cortex. *Neuron* 65, 472–479.
- Ostroff, L.E., Cain, C.K., Bedont, J., Monfils, M.H., and LeDoux, J.E. (2010). Fear and safety learning differentially affect synapse size and dendritic translation in the lateral amygdala. *Proc. Natl. Acad. Sci. USA* 107, 9418–9423.
- Pan, B.X., Dong, Y., Ito, W., Yanagawa, Y., Shigemoto, R., and Morozov, A. (2009). Selective gating of glutamatergic inputs to excitatory neurons of amygdala by presynaptic GABA_B receptor. *Neuron* 61, 917–929.
- Pape, H.C., Narayanan, R.T., Smid, J., Stork, O., and Seidenbecher, T. (2005). Theta activity in neurons and networks of the amygdala related to long-term fear memory. *Hippocampus* 15, 874–880.
- Paré, D., and Collins, D.R. (2000). Neuronal correlates of fear in the lateral amygdala: multiple extracellular recordings in conscious cats. *J. Neurosci.* 20, 2701–2710.
- Paré, D., and Gaudreau, H. (1996). Projection cells and interneurons of the lateral and basolateral amygdala: distinct firing patterns and differential relation to theta and delta rhythms in conscious cats. *J. Neurosci.* 16, 3334–3350.
- Paré, D., Pape, H.C., and Dong, J. (1995). Bursting and oscillating neurons of the rat basolateral amygdaloid complex in vivo: electrophysiological properties and morphological features. *J. Neurophysiol.* 74, 1179–1191.
- Paré, D., Collins, D.R., and Pelletier, J.G. (2002). Amygdala oscillations and the consolidation of emotional memories. *Trends Cogn. Sci. (Regul. Ed.)* 6, 306–314.
- Pinault, D. (1996). A novel single-cell staining procedure performed in vivo under electrophysiological control: morpho-functional features of juxtacellularly labeled thalamic cells and other central neurons with biocytin or Neurobiotin. *J. Neurosci. Methods* 65, 113–136.
- Pitkänen, A., Pikkarainen, M., Nurminen, N., and Ylinen, A. (2000). Reciprocal connections between the amygdala and the hippocampal formation, perirhinal

- cortex, and postrhinal cortex in rat. A review. *Ann. N Y Acad. Sci.* 917, 369–391.
- Popa, D., Duvarci, S., Popescu, A.T., Léna, C., and Paré, D. (2010). Coherent amygdalocortical theta promotes fear memory consolidation during paradoxical sleep. *Proc. Natl. Acad. Sci. USA* 107, 6516–6519.
- Pouille, F., and Scanziani, M. (2001). Enforcement of temporal fidelity in pyramidal cells by somatic feed-forward inhibition. *Science* 293, 1159–1163.
- Rainnie, D.G., Mania, I., Mascagni, F., and McDonald, A.J. (2006). Physiological and morphological characterization of parvalbumin-containing interneurons of the rat basolateral amygdala. *J. Comp. Neurol.* 498, 142–161.
- Richardson, M.P., Strange, B.A., and Dolan, R.J. (2004). Encoding of emotional memories depends on amygdala and hippocampus and their interactions. *Nat. Neurosci.* 7, 278–285.
- Royer, S., Sirota, A., Patel, J., and Buzsáki, G. (2010). Distinct representations and theta dynamics in dorsal and ventral hippocampus. *J. Neurosci.* 30, 1777–1787.
- Sangha, S., Narayanan, R.T., Bergado-Acosta, J.R., Stork, O., Seidenbecher, T., and Pape, H.C. (2009). Deficiency of the 65 kDa isoform of glutamic acid decarboxylase impairs extinction of cued but not contextual fear memory. *J. Neurosci.* 29, 15713–15720.
- Schumacher, J.W., Schneider, D.M., and Woolley, S.M. (2011). Anesthetic state modulates excitability but not spectral tuning or neural discrimination in single auditory midbrain neurons. *J. Neurophysiol.* 106, 500–514.
- Seidenbecher, T., Laxmi, T.R., Stork, O., and Pape, H.C. (2003). Amygdalar and hippocampal theta rhythm synchronization during fear memory retrieval. *Science* 301, 846–850.
- Singer, W. (1999). Neuronal synchrony: a versatile code for the definition of relations? *Neuron* 24, 49–65, 111–125.
- Smith, Y., Paré, J.F., and Paré, D. (2000). Differential innervation of parvalbumin-immunoreactive interneurons of the basolateral amygdaloid complex by cortical and intrinsic inputs. *J. Comp. Neurol.* 416, 496–508.
- Somogyi, P. (2010). Hippocampus: intrinsic organization. In *Handbook of Brain Microcircuits*, G.M. Shepherd and S. Grillner, eds. (Oxford: Oxford University Press), pp. 148–164.
- Sosulina, L., Graebenitz, S., and Pape, H.C. (2010). GABAergic interneurons in the mouse lateral amygdala: a classification study. *J. Neurophysiol.* 104, 617–626.
- Spampanato, J., Polepalli, J., and Sah, P. (2011). Interneurons in the basolateral amygdala. *Neuropharmacology* 60, 765–773.
- Tukker, J.J., Fuentealba, P., Hartwich, K., Somogyi, P., and Klausberger, T. (2007). Cell type-specific tuning of hippocampal interneuron firing during gamma oscillations in vivo. *J. Neurosci.* 27, 8184–8189.
- Windels, F., Crane, J.W., and Sah, P. (2010). Inhibition dominates the early phase of up-states in the basolateral amygdala. *J. Neurophysiol.* 104, 3433–3438.
- Woodruff, A.R., and Sah, P. (2007). Networks of parvalbumin-positive interneurons in the basolateral amygdala. *J. Neurosci.* 27, 553–563.
- Woodruff, A.R., Monyer, H., and Sah, P. (2006). GABAergic excitation in the basolateral amygdala. *J. Neurosci.* 26, 11881–11887.
- Woodruff, A.R., McGarry, L.M., Vogels, T.P., Inan, M., Anderson, S.A., and Yuste, R. (2011). State-dependent function of neocortical chandelier cells. *J. Neurosci.* 31, 17872–17886.
- Zar, J.H. (1999). *Biostatistical Analysis* (Upple Saddle River, NJ: Prentice Hall).

Supplemental Information

Cell-Type-Specific Recruitment of Amygdala

Interneurons to Hippocampal Theta Rhythm

and Noxious Stimuli In Vivo

Thomas C.M. Bienvenu, Daniela Busti, Peter J. Magill, Francesco Ferraguti, and Marco Capogna

INVENTORY OF SUPPLEMENTAL INFORMATION

Contains 9 Supplemental Figures, 7 Supplemental Tables, Supplemental Experimental Procedures, and Supplemental references.

- **Figure S1, linked to Figures 1, 2, 3, 4 and 6:** Somata locations of the recorded neurons in the basolateral amygdala. This figure shows that neurons were recorded throughout the BLA, and that subnuclei specificities cannot account for functional heterogeneities among cells of a type.
- **Figure S2, linked to Figures 1-5:** Firing relationships of individual BLA interneurons with hippocampal theta oscillations.
- **Figure S3, linked to Figures 1-4:** Firing relationships of BLA interneuron types with hippocampal gamma oscillations. This figure shows that none of the four interneuron types displayed firing modulation by dCA1 gamma oscillations (30-80 Hz).
- **Figure S4, linked to Figures 1-5:** Firing responses of individual BLA interneurons to hindpaw pinches.
- **Figure S5, linked to Figures 1-5:** Firing responses of individual BLA interneurons to electrical footshocks.

Figures S2, S4 and S5 show the electrophysiological results obtained for each interneuron, and illustrate how the main conclusions were reached.

- **Figure S6, linked to Figures 2-4:** Postsynaptic target analysis. This figure illustrates extensively the method used to identify postsynaptic targets of BLA interneurons at electron microscopic level. In panel (E), the diameters of dendrites targeted by various cell types are compared.
- **Figure S7, (A) linked to Figure 2, (B) linked to Figure 4:** Rostro-caudal extent of BLA interneurons. Represents for the first time entire views of BLA interneurons, an information necessary to unambiguously define cell types.

- **Figure S8, linked to Figure 6:** Extracellular spike waveform analysis. This figure shows that the four types of BLA interneurons could not be separated on the basis of their spike shapes. In contrast, GABAergic interneurons fired shorter action potentials than principal glutamatergic cells, as confirmed with unsupervised cluster analysis.

- **Figure S9, linked to Figure 7:** Spectral characteristics of local field potentials recorded in dorsal and ventral hippocampus and amygdala. This figure shows that LFP theta oscillations could be recorded in dCA1 and ventral hippocampus, but not in amygdala. Theta oscillations were robust and continuous only in dCA1.

- **Table S1, linked to Figures 1-4:** Neuronal domains innervated by interneurons of the BLA. This table contains detailed results of the electron microscopic analysis.

- **Table S2, linked to Figures 1-4:** Postsynaptic targets and neurochemical content of *in vivo*-recorded GABAergic neurons. This table gives detailed results of light microscopic analysis.

- **Table S3, linked to Figures 1-4 and Figure S3:** Analysis of dCA1 gamma modulation of BLA interneuron's spiking. This table contains the results obtained for each interneuron.

- **Table S4, linked to Figure 6:** Principal cells: electrophysiological and immunocytochemical analysis. This table contains results of immunohistochemical and electrophysiological analysis for each principal neuron.

- **Table S5, linked to Figure 6 and Figure S8:** Spike waveform parameters of all GABAergic and principal neurons. This table summarizes the values measured for every parameter in each of the 51 cells reported in this paper.

- **Table S6, linked to Figure 7:** Theta phase modulation of BLA neuron firing assessed with dorsal and ventral hippocampal references. This table recapitulates how the data plotted in Figure 7D were obtained. Moreover, it shows that LFP theta phase in ventral hippocampus varies between experiments by as much as 68.3° relative to dCA1 theta.

- **Table S7:** Primary antibodies used. This table explains how antibodies were obtained, diluted, and their specificity verified.

Supplemental Experimental Procedures describe recordings and analyses of ventral hippocampal theta and BLA principal neurons, anatomical methods, as well as the procedures followed to study CA1 gamma oscillations and spike waveforms.

Somata locations of the recorded neurons in the basolateral amygdala.

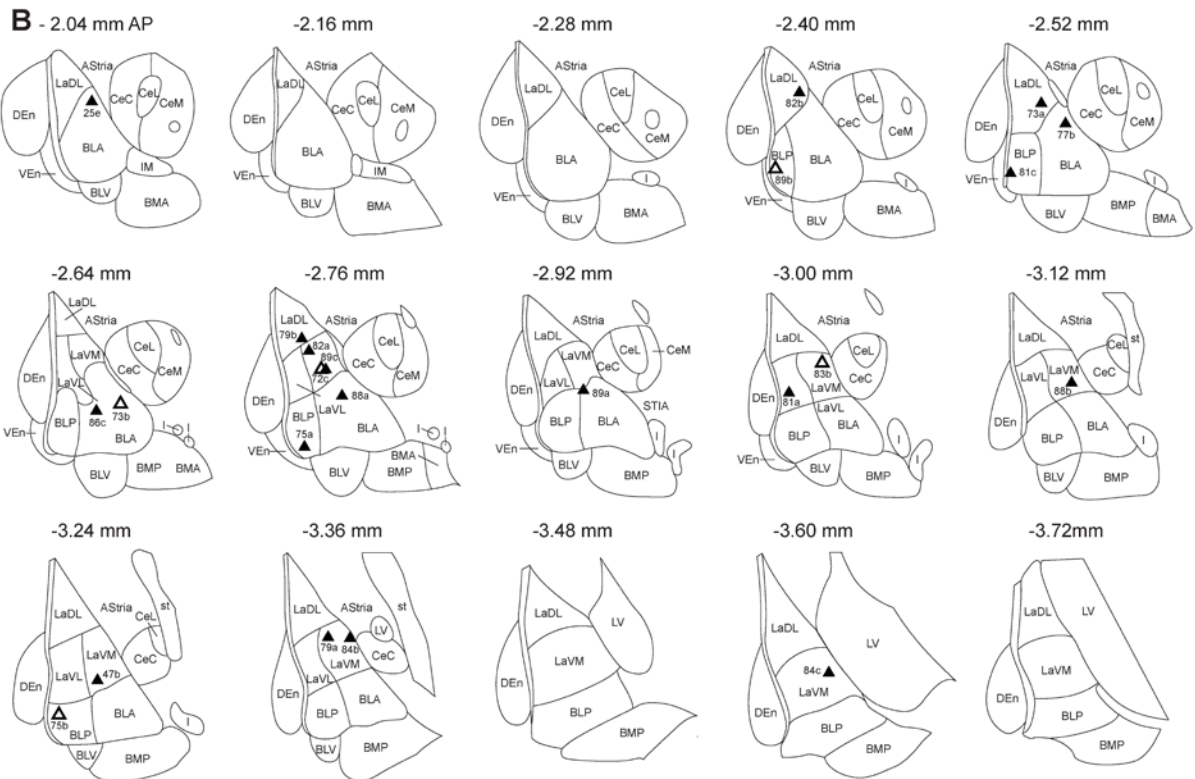
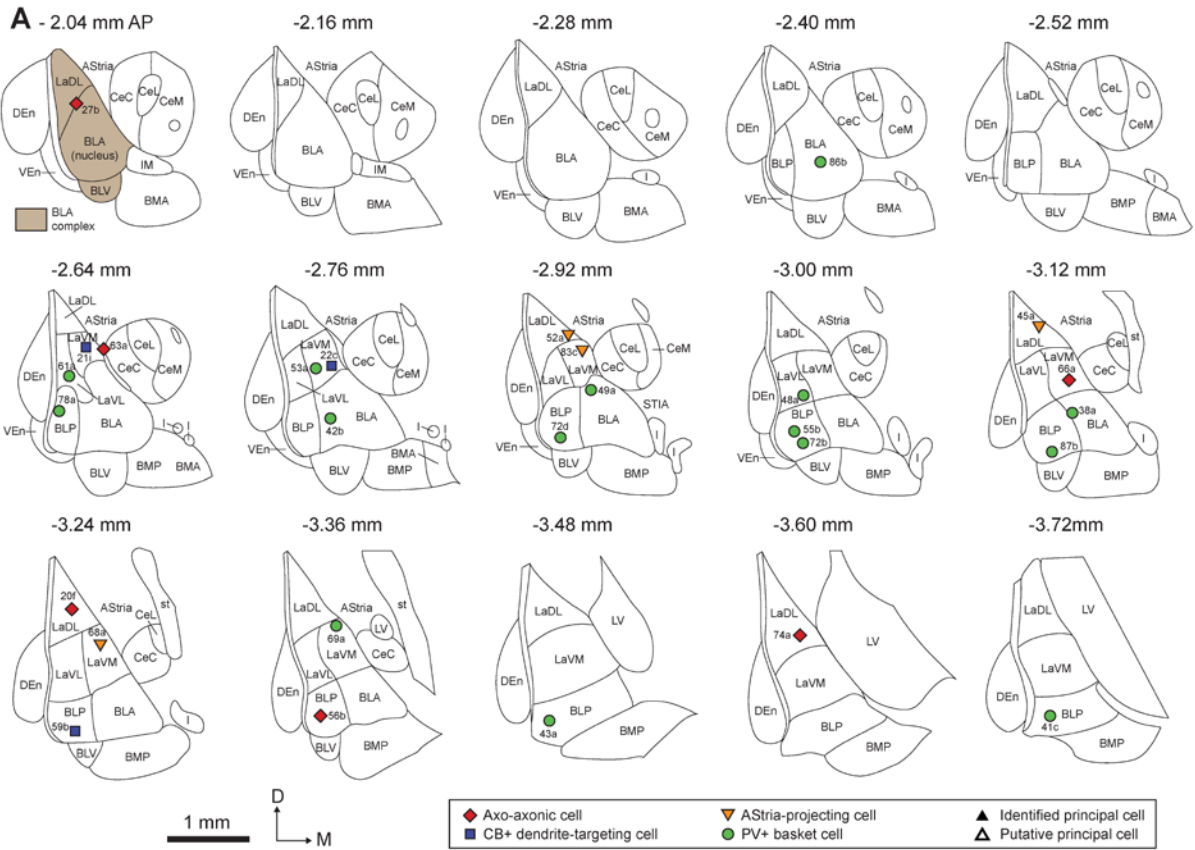


Figure S1. Somata locations of the recorded neurons in the basolateral amygdala (related to Figures 1-4 and 6).

Each symbol represents the position of a recorded neuron's soma in schematic coronal sections of the rat amygdala. The prefix "tjx" was removed from the experimental codes of neurons for clarity. Nomenclature and anatomical boundaries follow those of the *Rat brain in stereotaxic coordinates* (Paxinos and Watson, 2007). Distances above each panel represent the antero-posterior position (AP) of the corresponding coronal plane relative to the bregma junction (according to Paxinos and Watson, 2007). **(A)** Positions of the anatomically-identified GABAergic cells' somata. Except the basal ventral nucleus (BLV), our recordings covered all subdivisions of the amygdaloid basolateral complex. **(B)** Locations of the anatomically-identified and putative principal glutamatergic neurons recorded. Positions of putative principal neurons were extrapolated back from the documented distance to a labeled neuron in the same electrode track. D: dorsal, M: medial. Adapted with permission from Paxinos and Watson (2007).

Firing relationships of individual BLA interneurons with hippocampal theta oscillations.

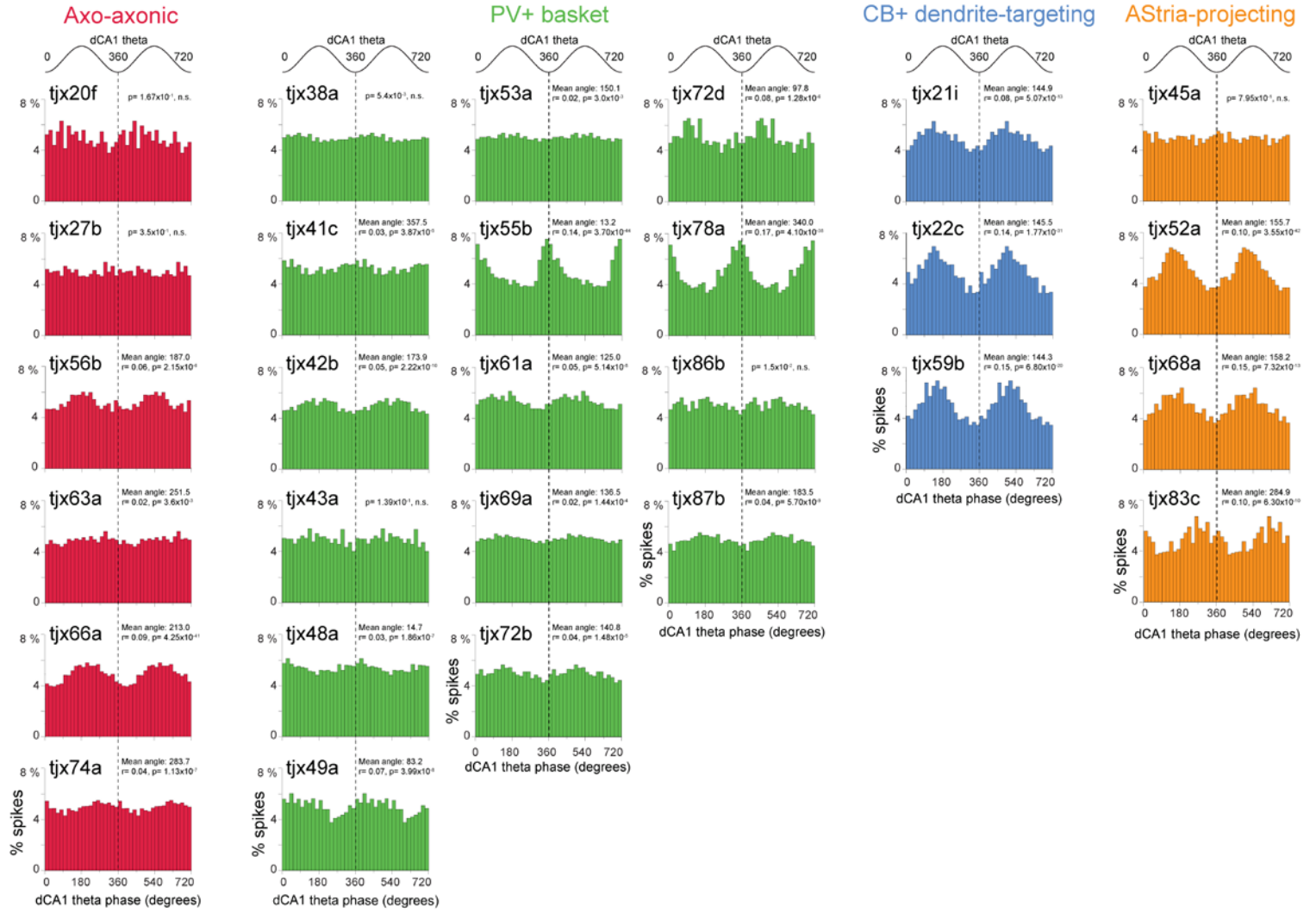


Figure S2. Firing relationships of individual BLA interneurons with hippocampal theta oscillations (related to Figures 1-5).

Phase histograms showing the spike distribution of each interneuron relative to hippocampal theta cycles, constructed from the entire dCA1 theta oscillations periods. Some neurons displayed a strong preference for a specific phase of the theta cycle (e.g., the CB+ dendrite-targeting cell tjx22c). The firing of some neurons showed only a small coupling to the theta rhythm (e.g., the PV+ basket cell tjx48a). The firing of other neurons was not significantly modulated (e.g. the axo-axonic cell tjx27b).

Homogeneity of phase locking was only observed for CB+ dendrite-targeting cells, a finding confirmed by statistical analysis (Moore test, see Results). In contrast, heterogeneity was observed for the other interneuron types, e.g. in PV+ basket cells. Mean angle, p values (Rayleigh test) and modulation depths are indicated for each cell. Two theta cycles are represented for clarity. 0°, 360° and 720°: theta troughs. Bin size of the histograms: 18°.

Firing relationships of BLA interneuron types with hippocampal gamma oscillations.

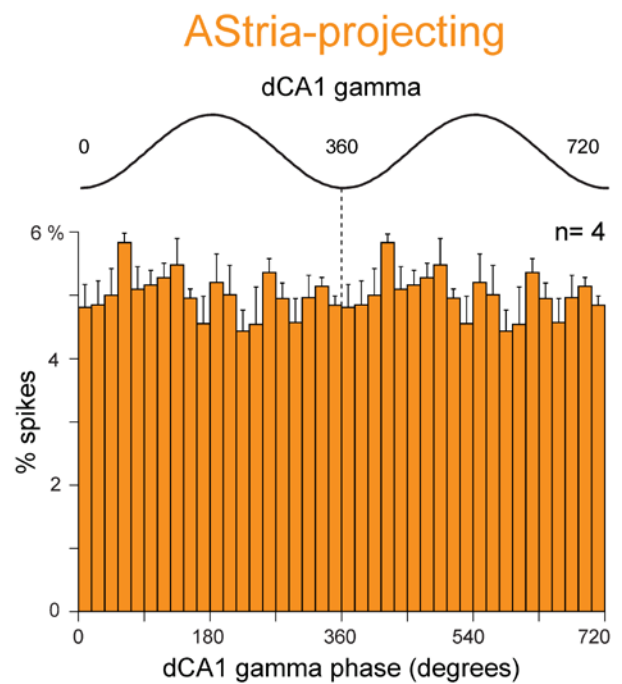
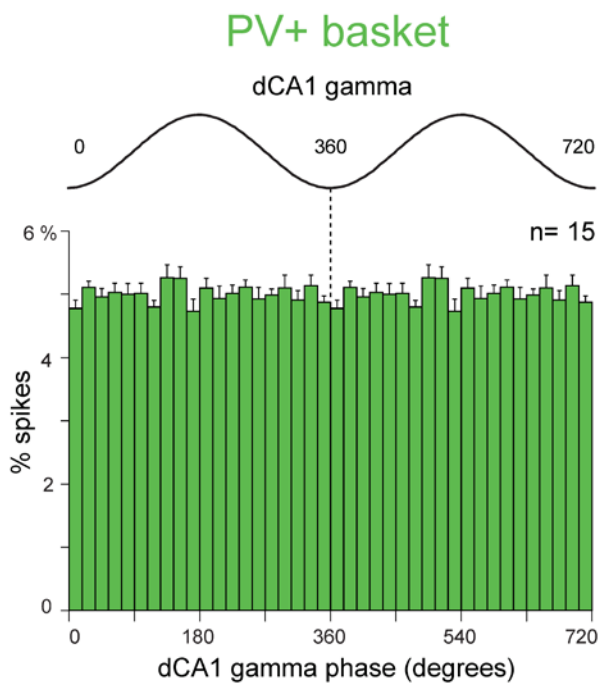
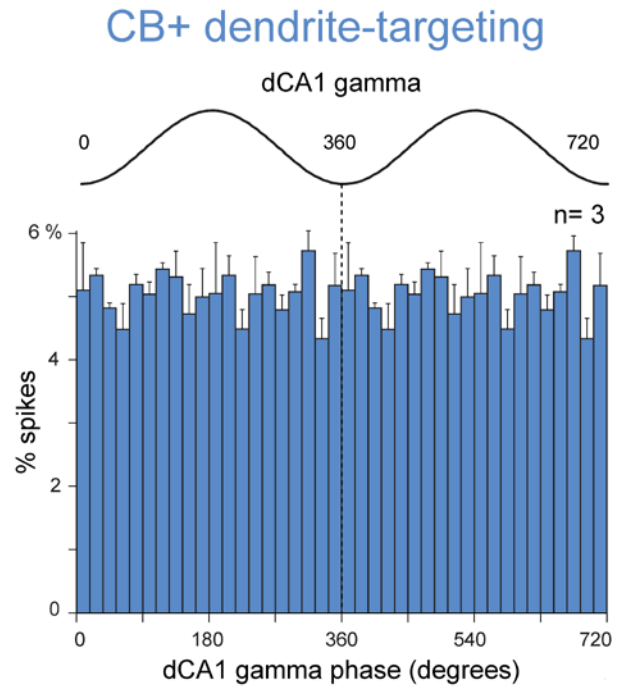
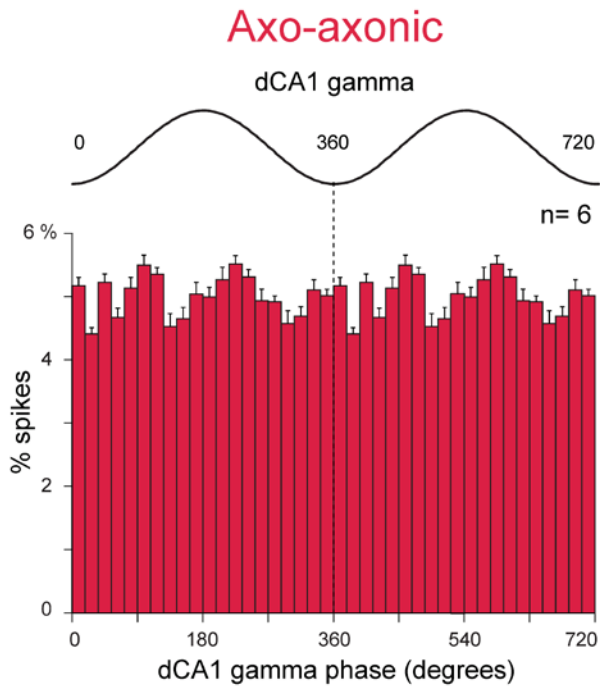


Figure S3. Firing relationships of BLA interneuron types with hippocampal gamma oscillations (related to Figures 1-4).

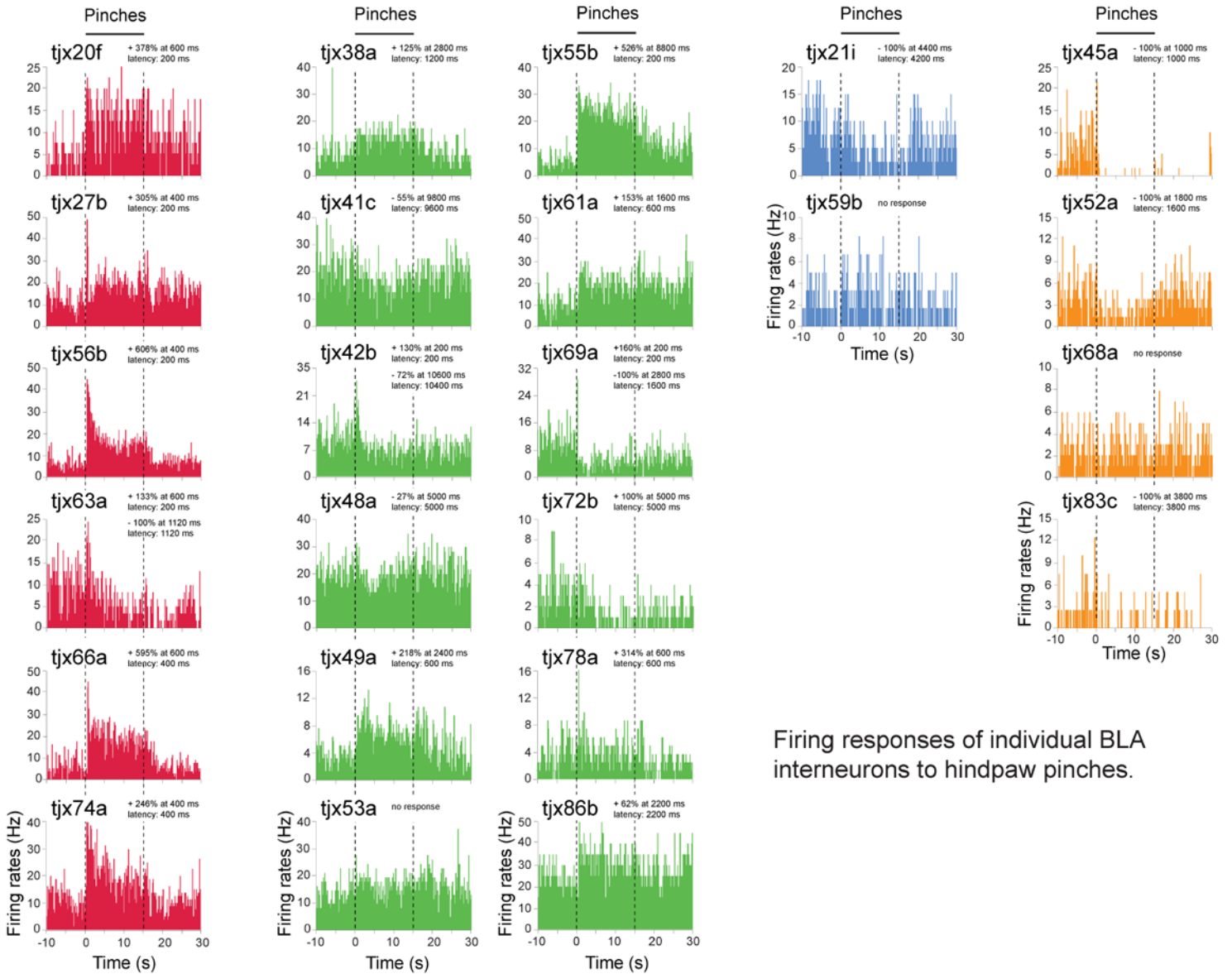
The firing of BLA interneurons is not modulated in phase with dCA1 gamma oscillations. This figure shows results obtained with the analysis of gamma oscillations (30-80 Hz) nested in dCA1 theta oscillations (3-6 Hz). Phase histograms (18° bins) represent mean spike timing of BLA interneuron types relative to gamma oscillation troughs (detected in dCA1 stratum oriens / pyramidale). Spike timing probability (%) in phase histograms was computed by dividing the number of action potentials in each bin by the total number of action potentials. No significant modulation was observed for the 28 interneurons (Rayleigh test). Similar results were obtained when analyses were performed on all gamma oscillation periods (regardless of their relationship to the theta rhythm). None of the 28 interneurons recorded in this study showed statistically significant modulation in phase with dCA1 gamma oscillations ($p > 0.005$, Rayleigh test). This held true for the analysis of theta-nested gamma oscillations, and for entire gamma oscillation periods (Table S3). This finding is consistent with gamma oscillations being generated locally. Error bars: SEM.

Axo-axonic

PV+ basket

CB+ dendrite-targeting

AStria-projecting



Firing responses of individual BLA interneurons to hindpaw pinches.

Figure S4. Firing responses of individual BLA interneurons to hindpaw pinches (related to Figures 1-5).

Peristimulus histograms showing spiking frequencies before, during and after hindpaw pinches for each interneuron recorded. Axo-axonic neurons and AStria-projecting cells responded relatively homogeneously to hindpaw pinches. In contrast, PV+ basket cells displayed heterogeneous responses, as recapitulated in their group average (see Figure 5). Latency of responses, and percentage and time of occurrence of maximal firing changes after pinches are indicated for each graph. Bin size of the histograms: 200 ms.

Firing responses of individual BLA interneurons to electrical footshocks.

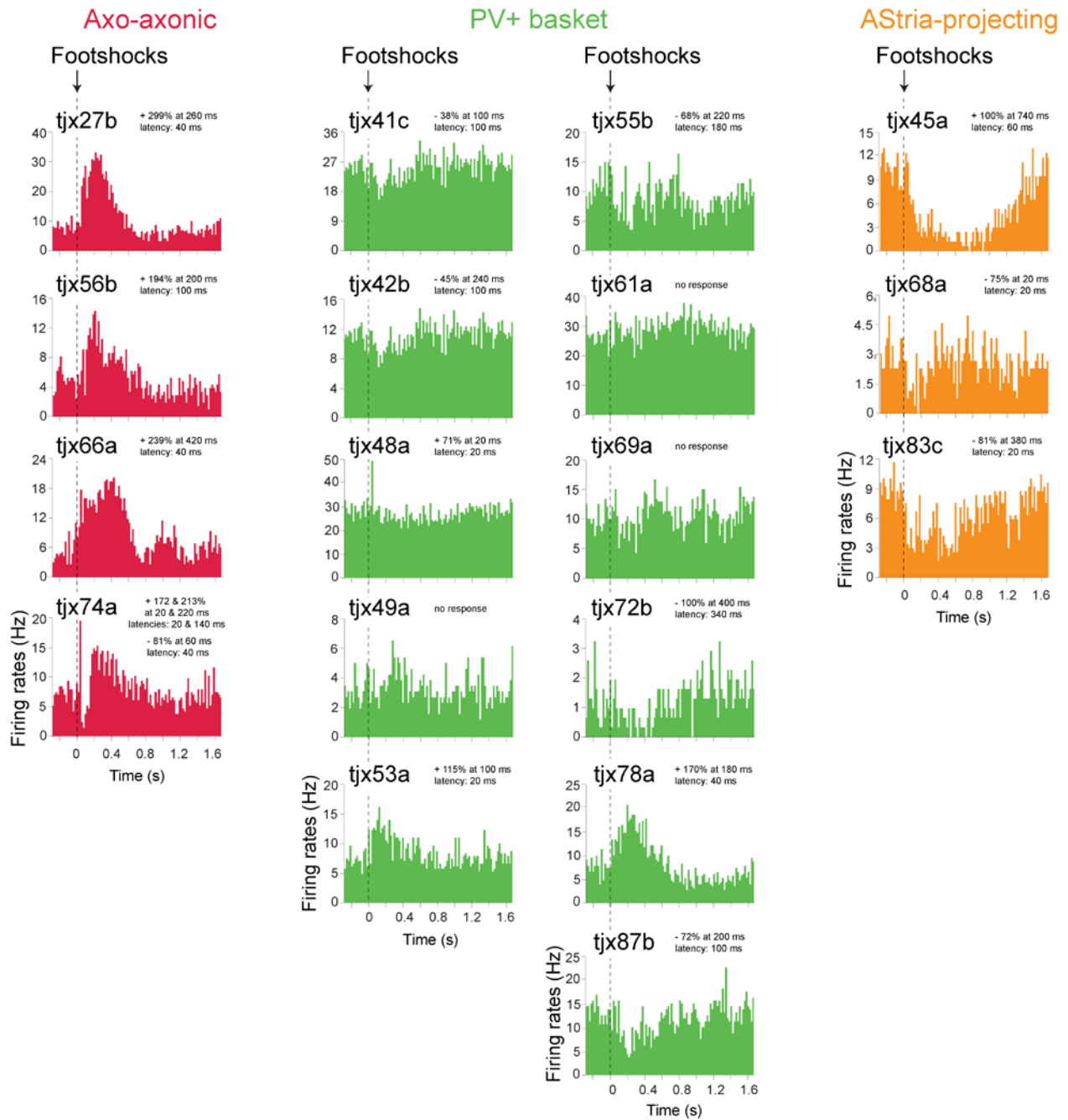


Figure S5. Firing responses of individual BLA interneurons to electrical footshocks (related to Figures 1-5).

Peristimulus histograms showing spiking frequencies before, during and after electrical footshocks for each interneuron recorded. Response patterns were similar to those observed with hindpaw pinches. All axo-axonic cells increased their firing frequency upon electrical footshocks, AStria-projecting cells were inhibited, whereas PV+ basket cells responded moderately and heterogeneously. Percentage, latency and time of occurrence of maximal firing changes after footshocks are indicated for each graph. Bin size of the histograms: 20 ms.

Postsynaptic target analysis.

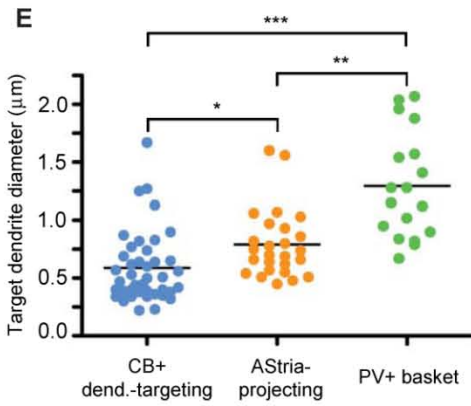
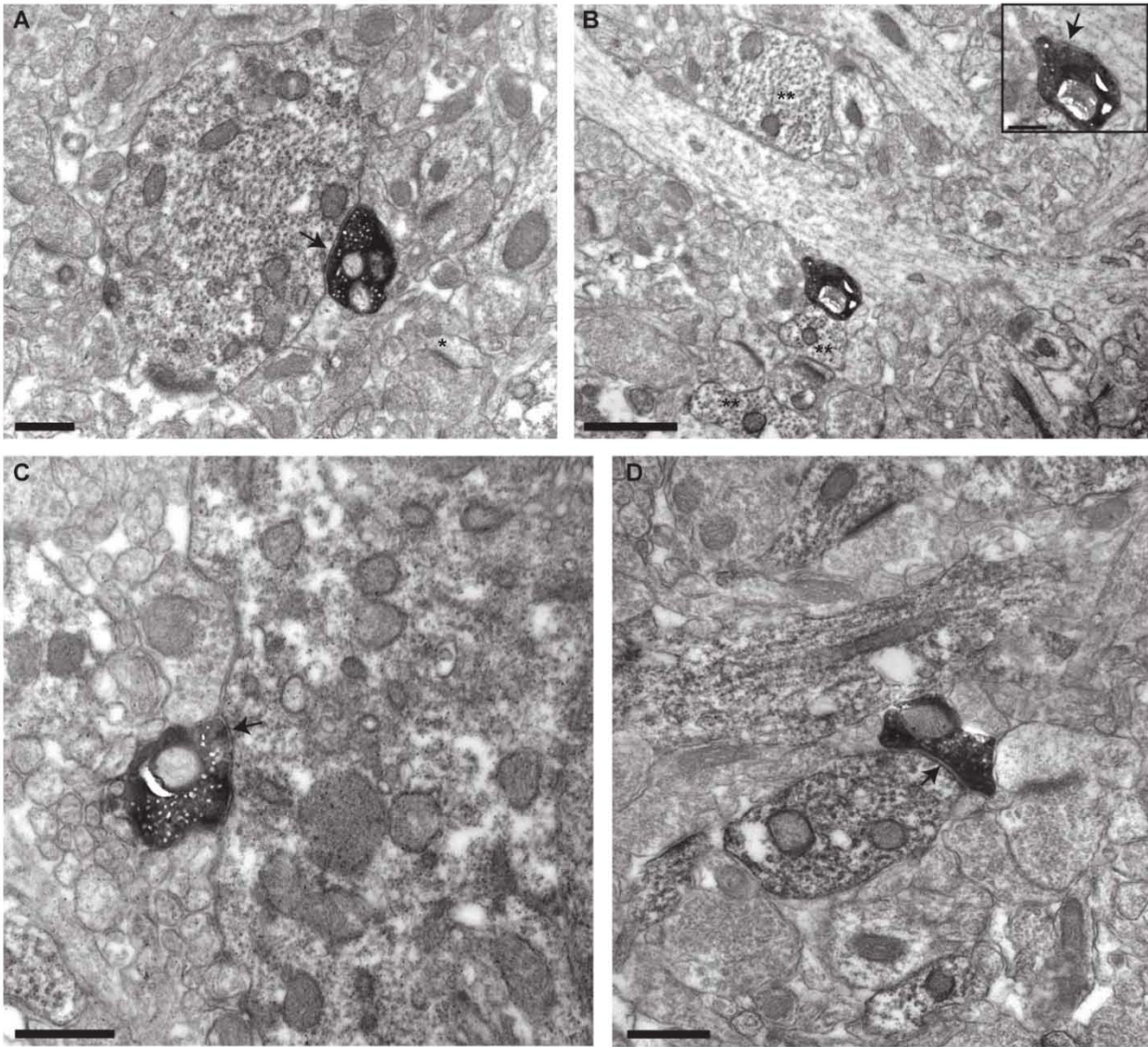


Figure S6. Postsynaptic target analysis (related to Figures 2-4).

Axonal boutons of Neurobiotin-filled neurons were visualized by HRP reaction using nickel-intensified DAB as a chromogen. This reaction resulted in a highly electron-opaque cytoplasmic precipitate sparing synaptic vesicles and mitochondria. Arrows indicate synaptic junctions. To determine if postsynaptic profiles were processes of glutamatergic principal neurons, we used anti-CaMKII α immunoperoxidase. This method appears specific and sensitive for principal neurons (see Supplemental Experimental Procedures). However, many more small dendrites and dendritic spines than expected were unlabeled (potentially false negatives; see panels A and B; *: unlabeled spine making an asymmetrical synapse with a nearby axonal bouton). Thus, under our experimental conditions, the lack of CaMKII α immunoperoxidase labeling did not allow to exclude that the postsynaptic target was a principal cell. As a possible explanation, we observed that some anatomically-identified glutamatergic neurons expressed low levels of CaMKII α (Figure 6C), that could not be detected in their dendrites using immunofluorescence.

(A) Symmetric (Gray's Type-II) synaptic junction formed by a PV⁺ basket cell (tjx49a) bouton with a large dendrite of a CaMKII α ⁺ neuron in BLA, identified by a fine electron-opaque HRP reaction product (using non-intensified DAB as chromogen).

(B) Type-II synaptic junction made by another bouton of tjx49a with a dendrite devoid of visible DAB product. Such postsynaptic target neuron remained unidentified. It could correspond to another GABAergic cell. Note the presence of clear DAB staining in nearby dendrites (**). The inset shows the synapse at higher magnification.

(C) Type-II synaptic junction formed by a third axonal bouton of tjx49 with the soma of an identified CaMKII α ⁺ principal neuron.

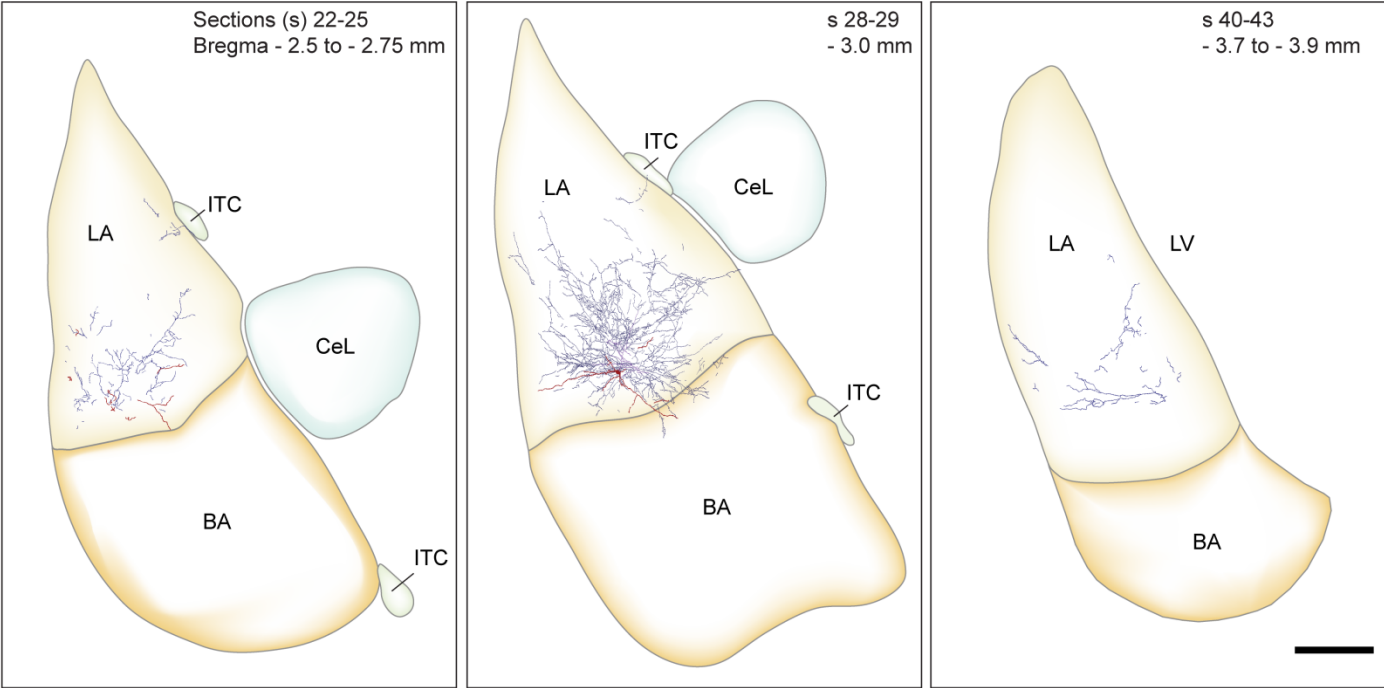
(D) Type-II synapse made by a bouton of an AStria-projecting neuron (tjx68a) with a dendrite of a CaMKII α ⁺ in the AStria. This target cell was a putative medium-sized spiny neuron, as we observed robust co-expression of CaMKII α and DARPP-32 in the AStria (see Figure 4E).

(E) Diameters of dendrites targeted by different interneuron types in the BLA. Circles represent individual measurements; horizontal bars represent mean values. Group differences were analyzed by the Kruskal-Wallis test followed by Dunn's post hoc analysis. *, $p < 0.05$, ** $p < 0.01$, *** $p < 0.005$.

Scale bars: (A) 1 μm ; (B) 1 μm , inset: 250 nm; (C,D) 500 nm.

Rostro-caudal extent of single BLA interneurons.

A. PV+ basket cell.



B. AStria-projecting cell.

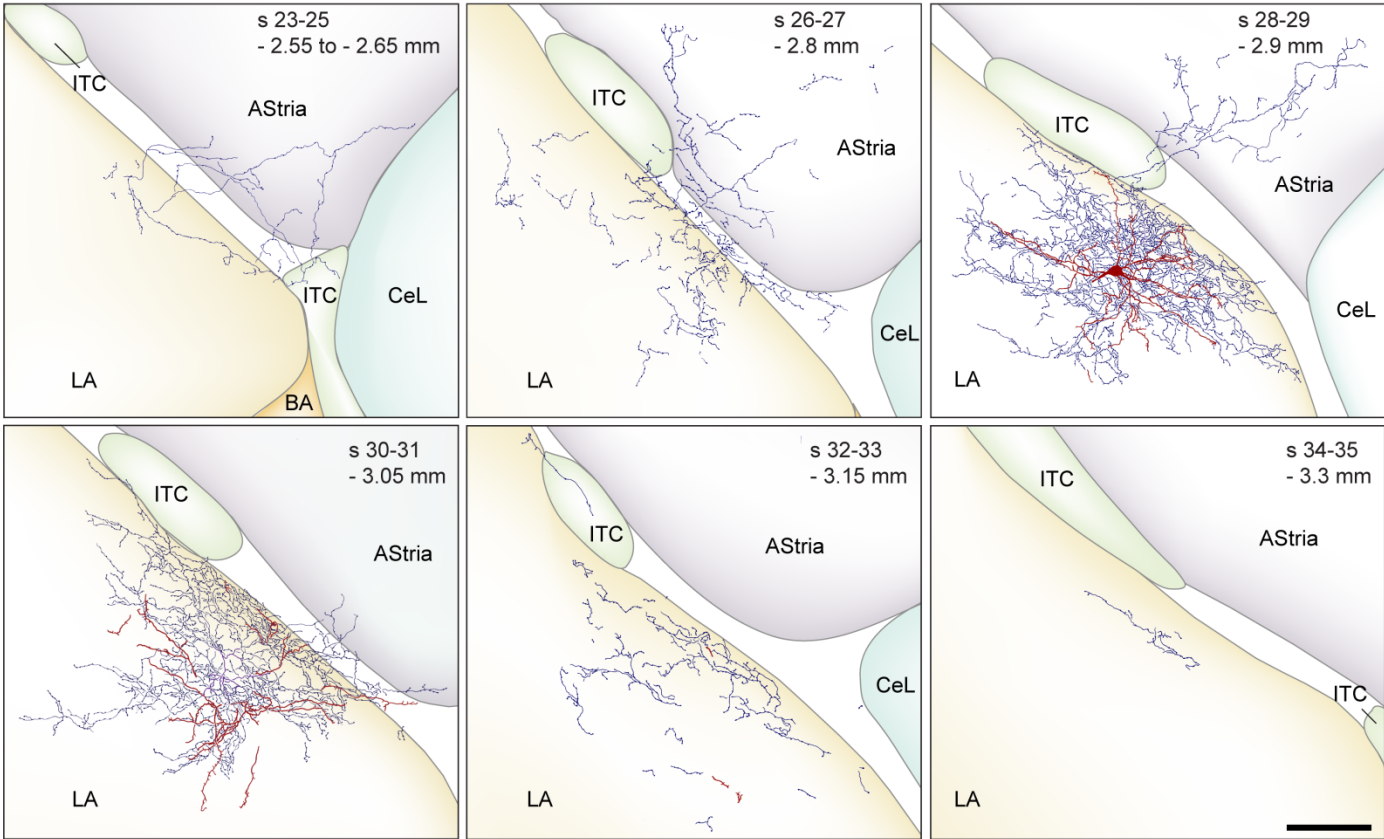


Figure S7. Rostro-caudal extent of single BLA interneurons (related to Figures 2 and 4).

Each panel shows the camera lucida reconstruction of dendrites (red) and axons (blue) from the corresponding subset of 60 μm -thick sections, at the indicated antero-posterior level (relative to bregma; following Paxinos and Watson, 2007).

(A) PV+ basket cell tjx48a (same cell as in Figure 2). The left panel shows the most rostral processes. The central panel depicts the section containing the soma and the section immediately caudal to it. The right panel illustrates the four sections before the last containing filled axon. The axon and dendrites of this cell covered a large portion of the BLA, in particular the lateral nucleus (axonal extent 1.4 mm anteroposterior). This example neuron was not unusual but in the upper size range. Such PV+ basket cells were the largest interneurons found in this study in terms of both dendritic and axonal spans. Dendritic and axonal trees of PV+ basket cells were stereotyped morphologically but varied proportionally in size. Large and small PV+ basket cell subtypes might exist, but we rather observed a size continuum (as suggested by McDonald and Betette, 2001).

(B) Reconstruction of the full dendritic and axonal fields of an AStria-projecting neuron (tjx52a; same cell as in Figure 4) from 13 sections (s23-s35; axonal extent: 780 μm rostrocaudal). In contrast to PV+ basket cells, dendrites of AStria-projecting cells never extended far from the soma. Likewise, their local axons were mostly confined to the dendritic field and were extraordinarily dense. Note that the projection to AStria was not merely the result of one axonal branch overlapping with BLA boundaries. On the contrary, it represented a significant part of the axonal arborisation and could be observed at several antero-posterior levels. An even larger axonal projection to AStria was observed in one neuron (tjx68a).

AStria: amygdala-striatum transition area, BA: basal amygdala, CeL: central lateral amygdaloid nucleus, ITC: intercalated cells cluster, LA: lateral amygdala, LV: lateral ventricle. Scale bars: (A) 250 μm , (B) 100 μm .

Extracellular spike waveform analysis.

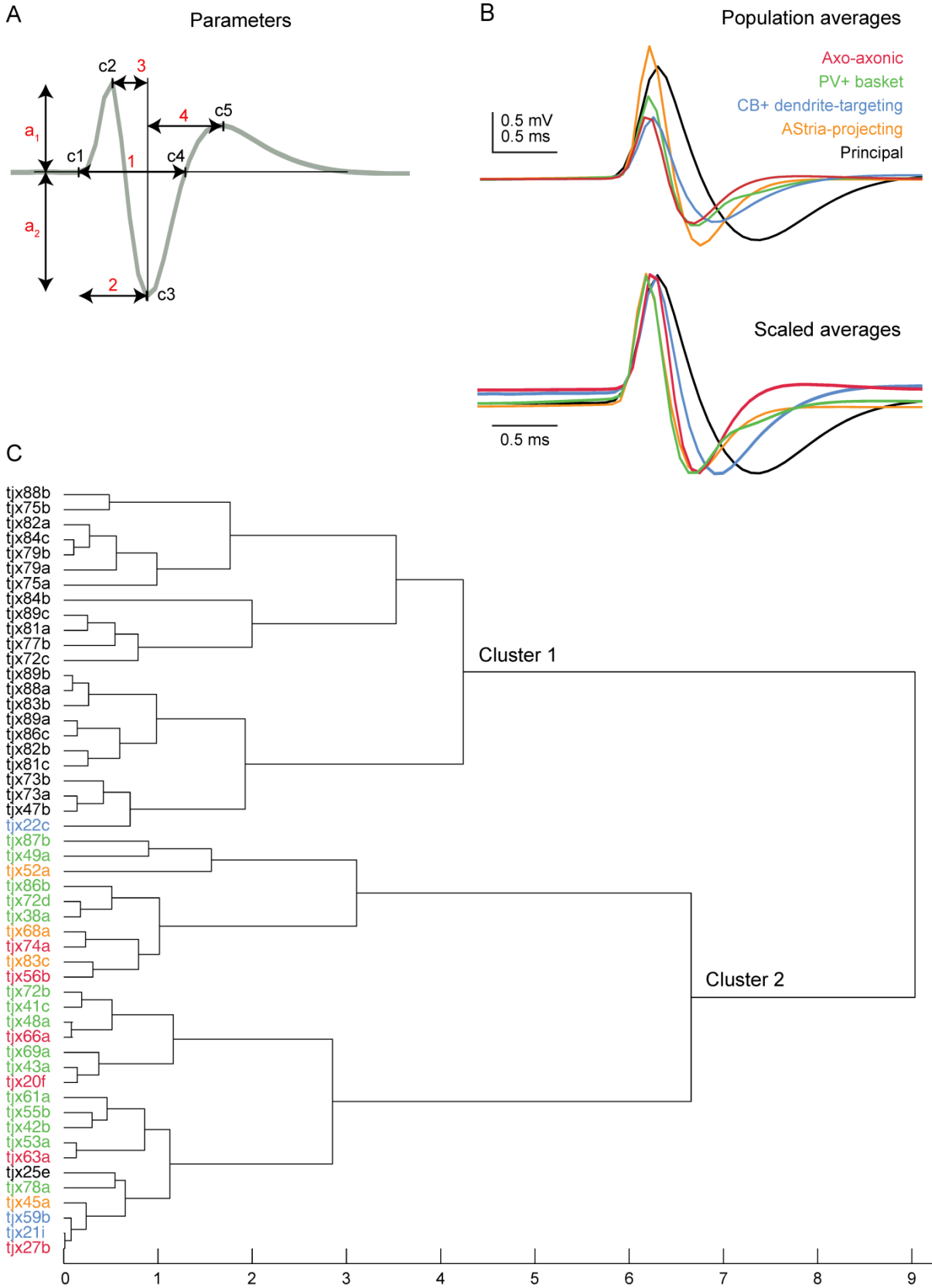


Figure S8. Extracellular spike waveform analysis (related to Figure 6).

This work identified for the first time BLA glutamatergic cells and interneurons recorded *in vivo*. Taking advantage of this, we investigated whether cell classes could be separated on the basis of their spike waveforms.

(A) Schematic of the parameters measured for each cell. 1: total width (c1-c4), 2: baseline to trough (c1-c3), 3: first peak to trough (c2-c3), 4: trough to second peak duration (c3-c5); a_1/a_2 : first peak / trough amplitude ratio. Cursors (c1-5) were placed as indicated in Supplemental Procedures. Measures made for each neuron are recapitulated in Table S5.

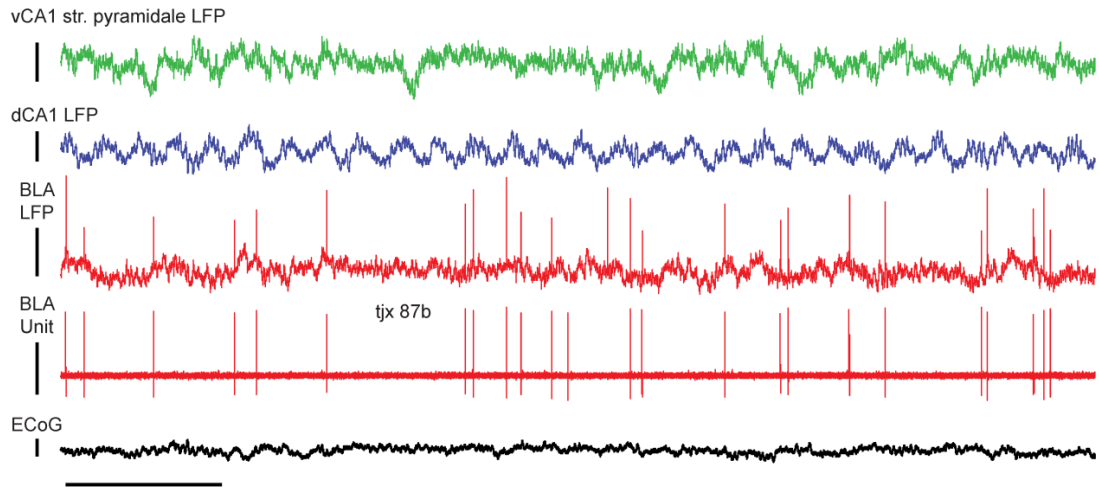
(B) Average spike waveform of each neuron class. Top: raw data, bottom: amplitude-scaled traces. Principal neurons fired longer-lasting spikes than interneurons as a group. Except trough to second peak duration, all spike width parameters were smaller for interneurons ($p < 0.0001$, Mann-Whitney U-test). The 1st peak/trough amplitude ratio did not differ between interneurons and principal cells ($p > 0.1$, Mann-Whitney U-test). None of the five parameters analyzed showed significant differences across interneuron types ($p > 0.05$, Kruskal Wallis test).

(C) Representative cluster analysis of spike waveforms. Cluster analyses using the various spike waveform parameters isolated two clusters, formed by interneurons and principal cells (here: cluster 1 and cluster 2, respectively; only one principal cell in the interneuron cluster and vice versa). They also confirmed the lack of statistical separation across interneuron types. X-axis shows the squared Euclidian distance between group centroids. Colour code is the same as elsewhere in the paper.

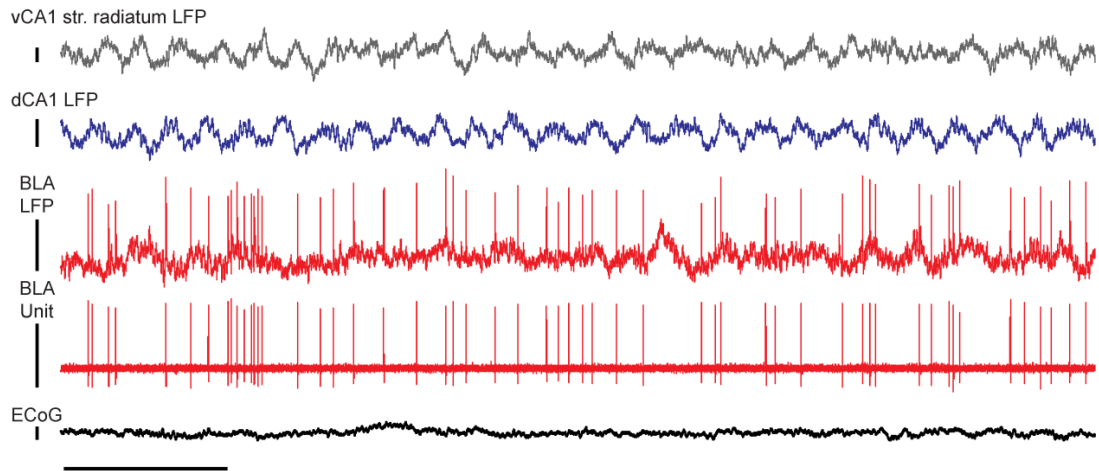
Our data suggest that spike shapes can be used to distinguish BLA interneurons and principal cells recorded extracellularly *in vivo*. This important issue has remained a matter of debate so far, in the absence of unambiguous identification of the recorded neurons. The present results are consistent with an earlier work proposing a spike duration cut-off of 0.5 ms (measured from peak to trough) for putative BLA interneurons ((Likhtik et al., 2006), Table S5). However, we cannot exclude that BLA interneuron types we did not record might fire longer spikes.

Spectral characteristics of local field potentials recorded in dorsal and ventral hippocampus and amygdala.

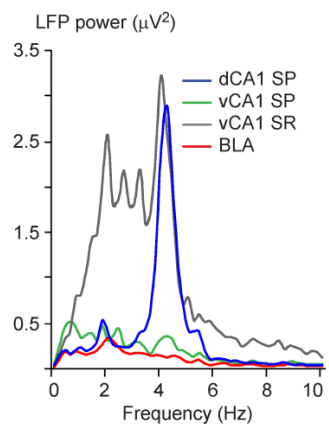
A



B



C



D

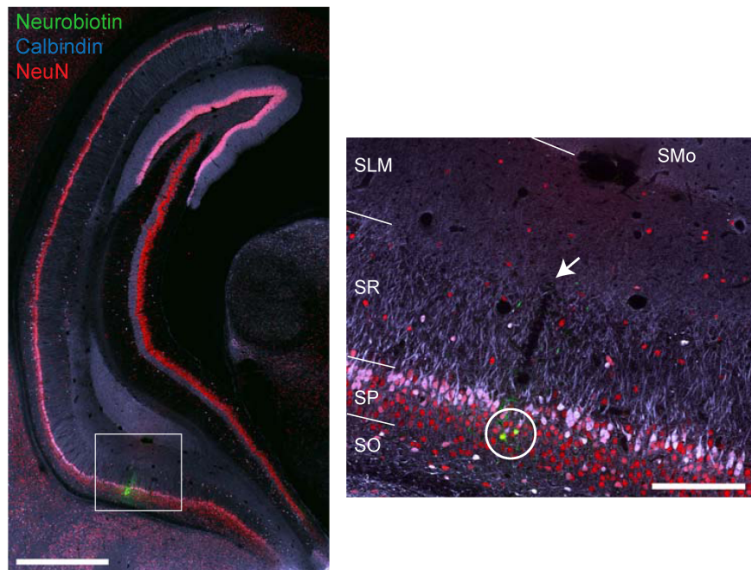


Figure S9. Spectral characteristics of local field potentials recorded in dorsal and ventral hippocampus and amygdala (related to Figure 7).

This figure shows typical data obtained with triple BLA, dCA1 and vCA1 recordings. In this experiment, LFP references were recorded in dorsal and ventral hippocampus, and a PV+ basket cell (tjx87b) was recorded in the BLA, during cortical activation (characterized by low amplitude, high frequency oscillations in the ECoG signal (Mallet et al., 2008)). No prominent theta oscillations were observed in str. pyramidale of vCA1 or in the BLA LFPs. In contrast, intermittent, but large amplitude theta oscillations could be recorded in vCA1 str. radiatum.

(A,B) Original data. LFPs: 0.3-300 Hz in this experiment. In **A**, the vCA1 reference electrode was located in str. pyramidale. **(B)** Keeping the single BLA unit recording stable, the vCA1 electrode was moved to str. radiatum (retracted by 355 μm).

(C) Corresponding power spectra of LFP signals. The dCA1 LFP shows a clear peak at ~ 4 Hz, indicating robust theta oscillations. LFPs of vCA1 str. pyramidale and BLA have no power peak in the theta range (3-6 Hz). LFP of vCA1 str. radiatum displays peaks at ~ 4 Hz, as well as lower frequencies (consistent with intermittent theta oscillations). SP: str. pyramidale; SR, str. radiatum.

(D) Structured illumination images showing the anatomically-confirmed recording sites in vCA1 from the same experiment. The white circle highlights the Neurobiotin (green) deposit made at the str. pyramidale recording site. NeuN immunoreactivity (red) was used as a pan-neuronal nuclear and cytoplasmic marker to delineate str. pyramidale. Calbindin immunoreactivity (light blue) highlights hippocampal layers. Colocalization with NeuN is indicated by white and pink. Right: higher magnification of the area delineated in the left panel. Arrow: recording site in str. radiatum, close to the str. lacunosum moleculare border. SO: str. oriens; SP: str. pyramidale; SR, str. radiatum; SLM: str. lacunosum moleculare; SMO: str. moleculare, dentate gyrus. Scale bars: (A,B) time: 1 s, LFPs: 0.5 mV, ECoG: 0.25 mV, unit tjx87: 1.5 mV; (D) left: 1 mm, right: 200 μm .

Cell type	Axo-axonic		PV+ basket		CB+ dendrite-targeting		AStria-projecting	
Cell code	tjx20f	tjx66a	tjx43a	tjx49a	tjx22c	tjx59b	tjx52a	tjx68a
Postsynaptic target (<i>CaMKIIα</i> +)								
Soma	-	1	8 (7)	14 (12)	-	-	11 (1)	3 (2)
Dendrite	-	-	12 (7)	6 (3)	21 (5)	20 (5)	9 (4)	17 (7)
Axon initial segment	21	20*	-	-	-	-	-	-
Unidentified	-	1**	-	-	-	-	-	-
Total	21	22	20	20	21	20	20	20

Table S1. Neuronal domains innervated by interneurons of the BLA.

Postsynaptic target identity was determined using standard criteria (Peters et al., 1991). Synapses were analyzed in serial (3-10) ultrathin sections.

The table indicates the number of synapses found in the corresponding categories.

* One synapse was made with a dendritic axon hillock (segment from which emerged the axon initial segment, as defined in Peters et al., 1991).

** Since four investigators could not conclude whether the postsynaptic profile was part of an AIS or a dendrite, it was considered unidentified.

Recorded neurons		Postsynaptic targets				Molecular markers									
Cell type	Cell code	Ankyrin G+	CamKII α s and d	DARPP-32+	EM	Calbindin	CB1-R	Calretinin	GABA _A -R α 1	GAD	Kv 3.2	Nk1-R	PV	SOM	VGAT
Axo-axonic	tjx20f	AIS	n.t.	-	AIS	0 (d)	n.t.	n.t.	0 (s,d)	n.t.	n.t.	n.t.	1 (s,d)**	0 (s)	n.t.
	tjx27b	AIS	n.t.	-	n.t.	0 (d)	n.t.	0 (d)	0 (s,d)	n.t.	n.t.	n.t.	1 (d,ax)	n.t.	n.t.
	tjx56b	AIS	0	-	n.t.	0 (s)	n.t.	n.t.	1 (d)	n.t.	n.t.	n.t.	1 (d,ax)	n.t.	n.t.
	tjx63a	AIS	n.t.	-	n.t.	0 (d)	n.t.	n.t.	0 (d)	n.t.	n.t.	n.t.	1 (s,d,ax**)	n.t.	n.t.
	tjx66a	AIS	n.t.	-	AIS	0 (d)	n.t.	n.t.	1 (d)	n.t.	1 (s)	n.t.	1 (s,d,ax)	n.t.	n.t.
	tjx74a	AIS	n.t.	-	n.t.	0 (d)	n.t.	n.t.	0 (d)	n.t.	n.t.	n.t.	1 (d,ax)	n.t.	n.t.
PV+ basket	tjx38a	n.t.	n.t.	-	n.t.	1 (d)	n.t.	n.t.	1 (d)	n.t.	n.t.	n.t.	1 (d)	n.t.	n.t.
	tjx41c	n.t.	s, d	-	n.t.	1 (d)**	n.t.	n.t.	1 (d)	n.t.	n.t.	n.t.	1 (d,ax)	n.t.	n.t.
	tjx42b	n.t.	D, s	-	n.t.	1 (d,ax)	n.t.	n.t.	1 (d)	n.t.	n.t.	n.t.	1 (d,ax)	n.t.	n.t.
	tjx43a	0	s, d	-	s,d	1 (s,d,ax)	n.t.	n.t.	1 (d)	n.t.	n.t.	n.t.	1 (d,ax)	n.t.	n.t.
	tjx48a	n.t.	s, d	-	S,d	1 (d,ax)	n.t.	n.t.	1 (d)	n.t.	1 (s)	n.t.	1 (d,ax)	n.t.	n.t.
	tjx49a	n.t.	s, d	-	S,d	1 (d,ax)	n.t.	n.t.	1 (d)**	n.t.	n.t.	n.t.	1 (d,ax)	n.t.	n.t.
	tjx53a	n.t.	s, d	-	n.t.	1 (d,ax)	n.t.	n.t.	1 (d)	n.t.	n.t.	n.t.	1 (d)	n.t.	n.t.
	tjx55b	0	s, d	-	n.t.	1 (d,ax)	n.t.	n.t.	1 (d)	n.t.	n.t.	n.t.	1 (d,ax)	n.t.	n.t.
	tjx61a	0	s, d	-	n.t.	1 (d,ax)	n.t.	n.t.	1 (d)	n.t.	n.t.	n.t.	1 (d,ax)	n.t.	n.t.
	tjx69a	n.t.	s, d	-	n.t.	1 (d,ax)	n.t.	n.t.	1 (d)	n.t.	n.t.	n.t.	1 (d)	n.t.	n.t.
	tjx72b	n.t.	n.t.	-	n.t.	1 (s,d,ax)	n.t.	n.t.	1 (s,d)	n.t.	n.t.	n.t.	1 (s,d,ax)	n.t.	n.t.
	tjx72d	n.t.	n.t.	-	n.t.	1 (d,ax)	n.t.	n.t.	1 (d)	n.t.	n.t.	n.t.	1 (d,ax)	n.t.	n.t.
	tjx78a	n.t.	s, d	-	n.t.	1 (s)	n.t.	n.t.	1 (d)	n.t.	n.t.	n.t.	1 (d,ax)	n.t.	n.t.
	tjx86b	n.t.	s, d	-	n.t.	1 (d)	n.t.	n.t.	1 (d)	n.t.	n.t.	n.t.	1 (d)	n.t.	n.t.
tjx87b	n.t.	D, s	-	n.t.	1 (d)	n.t.	n.t.	1 (d)	n.t.	n.t.	n.t.	1 (d)	n.t.	n.t.	
CB+ dendrite-targeting	tjx21i	n.t.	d	-	n.t.	1 (s)	n.t.	n.t.	n.t.	n.t.	n.t.	n.t.	1 (s,d)**	0 (s,ax)	n.t.
	tjx22c	n.t.	d	-	D	1 (d)	0 (ax)	n.t.	0 (s,d)	n.t.	n.t.	0 (d)	1 (s)*	0 (s,ax)	1 (ax)
	tjx59b	n.t.	d	-	D	1 (d)	n.t.	n.t.	1 (s,d)	n.t.	n.t.	n.t.	n.t.	0 (s)	n.t.
AStria-projecting	tjx45a	n.t.	n.t.	n.t.	n.t.	1 (d)	0 (ax)	n.t.	1 (d)**	n.t.	n.t.	n.t.	1 (d,ax)	n.t.	1 (ax)
	tjx52a	n.t.	s,d*	s,d	S,d	0 (d)	n.t.	0 (d)	0 (d)	1 (ax)	n.t.	0 (s,d)	1 (d)	n.t.	1 (ax)
	tjx68a	n.t.	s,d*	s,d	s,D	0 (d)	n.t.	n.t.	0 (d)	n.t.	n.t.	n.t.	1 (d,ax**)	n.t.	n.t.
	tjx83c	n.t.	n.t.	n.t.	n.t.	1 (d)**	n.t.	n.t.	0 (d)	n.t.	n.t.	n.t.	1 (s,d,ax)**	n.t.	n.t.

Table S2. Postsynaptic targets and neurochemical content of *in vivo*-recorded GABAergic neurons.

Postsynaptic targets: *: in lateral amygdala and AStria. 0 indicates the corresponding principal cell compartment was not in apposition with labeled axon varicosities. AIS: axon initial segment, ax: axon, d: dendrites, s: soma; capital letter: main targets. EM column: postsynaptic targets verified with electron microscopy.

Molecular markers: **: weakly positive, brackets: cell domain tested for immunoreactivity. 0 indicates the cell was concluded immunonegative, 1 indicates the cell was concluded immunopositive. CaMKII α : Calcium/calmodulin dependent kinase II alpha subunit, CB1-R: cannabinoid receptor 1, DARPP-32: dopamine and cyclic adenosine 3',5'-monophosphate-regulated phosphoprotein with molecular weight of 32 kDa, GAD: glutamic acid decarboxylase, Nk1-R: neurokinin receptor 1, PV: parvalbumin, SOM: somatostatin, VGAT: vesicular GABA transporter.

Recorded neurons		Firing during dCA1 gamma nested in theta oscillations				Firing during dCA1 gamma, full recordings			
Cell type	Cell code	Mean angle	Modulation depth	p (Rayleigh)	n spikes	Mean angle	Modulation depth	p (Rayleigh)	n spikes
Axo-axonic	tjx20f	84.28	0.0253	0.878	202	88.75	0.0045	0.921	4130
	tjx27b	157.41	0.0405	0.218	929	251.54	0.0019	0.971	8377
	tjx56b	270.44	0.0244	0.412	1484	221.09	0.0100	0.430	8398
	tjx63a	222.25	0.0162	0.513	2532	213.39	0.0055	0.910	3099
	tjx66a	232.65	0.0269	0.102	3160	40.94	0.0055	0.951	1649
	tjx74a	68.78	0.0260	0.404	1345	223.63	0.0179	0.511	2094
PV+ basket	tjx38a	85.39	0.0253	0.117	3346	88.19	0.0078	0.800	3709
	tjx41c	153.20	0.0347	0.043	2613	205.47	0.0111	0.496	5688
	tjx42b	219.71	0.0063	0.901	2643	178.80	0.0238	0.096	4142
	tjx43a	235.37	0.0126	0.837	1120	141.69	0.0151	0.440	3626
	tjx48a	58.97	0.0050	0.887	4775	349.69	0.0266	0.043	4473
	tjx49a	328.40	0.0387	0.355	693	295.63	0.0104	0.537	5767
	tjx53a	253.44	0.0081	0.607	7684	237.82	0.0073	0.395	17507
	tjx55b	61.66	0.0068	0.958	913	28.85	0.0103	0.822	1848
	tjx61a	76.13	0.0096	0.713	3689	78.03	0.0087	0.358	13572
	tjx69a	113.46	0.0075	0.607	8911	144.17	0.0170	0.377	3393
	tjx72b	120.94	0.0251	0.239	2270	116.26	0.0073	0.573	10518
	tjx72d	24.18	0.0347	0.528	531	211.32	0.0172	0.111	7461
	tjx78a	215.22	0.0424	0.199	899	263.96	0.0091	0.435	10124
	tjx86b	210.76	0.0355	0.333	873	219.67	0.0060	0.601	13984
tjx87b	298.55	0.0149	0.774	1151	80.85	0.0146	0.374	4584	
CB+ dendrite-targeting	tjx21i	282.01	0.0021	0.995	996	106.73	0.0067	0.902	2285
	tjx22c	201.61	0.0080	0.934	1059	233.36	0.0065	0.790	5493
	tjx59b	60.46	0.0120	0.881	884	139.54	0.0177	0.135	6372
AStria-projecting	tjx45a	97.22	0.0224	0.401	1821	207.29	0.0086	0.754	3865
	tjx52a	91.77	0.0668	0.084	555	230.15	0.0287	0.044	3778
	tjx68a	0.59	0.0313	0.195	1674	27.63	0.0155	0.353	4346
	tjx83c	175.80	0.0211	0.611	1109	284.55	0.0129	0.340	6457

Table S3. Analysis of dCA1 gamma modulation of BLA interneuron's spiking.

Cell code	Firing during dCA1 theta oscillations						Neurochemical content		
	Rate (Hz)	CV	Mean angle	Angular deviation	p (Rayleigh)	Modulation depth	CamKII α	Calbindin	VGluT1
tjx23f	n.t.						1 (d)	1 (s)*	1 (ax)
tjx25e	0.63	1.25	n.s.	n.s.	7.7×10^{-1}	n.s.	n.t.	n.t.	1 (ax)
tjx47b	1.34	1.71	199.3	124.7	8.6×10^{-13}	0.09	1 (s)	1 (s)*	1 (ax)
tjx72c	0.50	2.26	186.9	93.0	2.4×10^{-26}	0.27	n.t.	n.t.	n.t.
tjx73a	0.06	2.43	n.s.	n.s.	8.2×10^{-1}	n.s.	1 (s)	1 (s)*	n.t.
tjx73b	0.06	2.25	323.7	98.7	2.0×10^{-10}	0.23	n.t.	n.t.	n.t.
tjx75a	0.44	2.00	n.s.	n.s.	9.0×10^{-1}	n.s.	1 (s)	1 (s)*	n.t.
tjx75b	0.33	1.22	302.0	103.0	3.1×10^{-11}	0.20	n.t.	n.t.	n.t.
tjx77b	0.19	2.22	n.s.	n.s.	7.9×10^{-2}	n.s.	1 (s)	0 (s)	1 (ax)
tjx79a	0.15	1.68	n.s.	n.s.	9.5×10^{-2}	n.s.	1 (s)	1 (s)*	1 (ax)
tjx79b	0.11	2.17	n.s.	n.s.	5.3×10^{-2}	n.s.	1 (s)	1 (s)*	1 (ax)
tjx81a	0.03	1.71	n.s.	n.s.	5.8×10^{-1}	n.s.	n.t.	1 (s)	1 (ax)
tjx81c	0.38	1.77	n.s.	n.s.	7.9×10^{-1}	n.s.	1 (s)	1 (s)*	1 (ax)
tjx82a	0.32	1.70	141.0	95.8	1.5×10^{-10}	0.25	1 (s)	1 (s)*	1 (ax)
tjx82b	0.29	2.52	n.s.	n.s.	3.9×10^{-1}	n.s.	1 (s)	0 (s)	1 (ax)
tjx83b	0.04	1.14	n.s.	n.s.	4.9×10^{-1}	n.s.	n.t.	n.t.	n.t.
tjx84b	0.19	1.95	n.s.	n.s.	4.7×10^{-1}	n.s.	1 (s)	1 (s)*	1 (ax)
tjx84c	0.03	1.34	n.s.	n.s.	3.1×10^{-1}	n.s.	1 (s)	1 (s)	1 (ax)
tjx86c	0.24	1.60	128.5	124.9	1.2×10^{-6}	0.09	1 (s)	0 (s)	1 (ax)
tjx88a	0.14	3.77	n.s.	n.s.	5.8×10^{-2}	n.s.	1 (s)	0 (s)	1 (ax)
tjx88b	0.13	2.73	n.s.	n.s.	1.9×10^{-1}	n.s.	1 (s)	0 (s)	n.t.
tjx89a	0.19	2.31	268.2	117.9	3.1×10^{-7}	0.12	1 (s)	0 (s)	1 (ax)
tjx89b	0.26	1.04	176.1	126.4	3.0×10^{-3}	0.09	n.t.	n.t.	n.t.
tjx89c	0.49	2.07	213.7	104.9	9.4×10^{-10}	0.19	1 (s)	1 (s)*	1 (ax)

Table S4. Principal cells: electrophysiological and immuno-cytochemical analysis.

0 indicates the cell was tested immunonegative, 1 indicates the cell was tested immunopositive. Brackets: cell domain tested for immunoreactivity. CaMKII α : Calcium/calmodulin dependant kinase II alpha subunit, CV: coefficient of variation of firing, VGluT1: vesicular glutamate transporter 1. *: weakly immunopositive. ax: axon, d: dendrites, s: soma. n.s. not statistically significant, n.t. not tested.

Recorded neurons			Spike duration parameters (ms)				Spike amplitude parameters	
Cell type	Cell code	n spikes	Total width (c1-c4)	Baseline-trough (c1-c3)	1st peak-through (c2-c3)	Trough-2nd peak (c3-c5)	1st peak/through (a1/a2)	Amplitude (a1+a2, mV)
Axo-axonic	tjx20f	1412	1.06	0.57	0.33	0.86	1.13	2.16
	tjx27b	8630	1.08	0.55	0.33	0.83	1.35	1.55
	tjx56b	6519	1.09	0.55	0.32	0.76	1.76	0.98
	tjx63a	8231	1.00	0.49	0.28	0.65	1.60	1.39
	tjx66a	16475	0.85	0.48	0.28	0.68	0.97	0.80
	tjx74a	10241	1.29	0.58	0.36	0.98	2.03	2.44
	average	8585	1.06	0.54	0.32	0.79	1.47	1.55
	s.e.m.	2007	0.06	0.02	0.01	0.05	0.16	0.26
PV+ basket	tjx38a	10829	1.92	0.59	0.39	n.a.	1.72	0.87
	tjx41c	7774	0.79	0.48	0.27	0.58	0.84	0.98
	tjx42b	11985	1.17	0.46	0.26	n.a.	1.45	2.18
	tjx43a	2971	1.20	0.58	0.36	0.93	1.12	1.37
	tjx48a	15545	0.86	0.45	0.29	0.69	0.95	1.13
	tjx49a	6962	0.92	0.41	0.24	n.a.	2.19	1.65
	tjx53a	24510	1.16	0.43	0.26	n.a.	1.57	1.98
	tjx55b	5758	1.20	0.47	0.29	0.85	1.33	1.76
	tjx61a	2209	0.78	0.41	0.24	0.53	1.23	1.46
	tjx69a	25166	1.16	0.62	0.40	0.95	1.03	1.89
	tjx72b	4125	0.73	0.46	0.27	0.53	0.76	0.95
	tjx72d	4046	2.32	0.65	0.42	n.a.	1.75	2.21
	tjx78a	4051	1.49	0.60	0.38	1.17	1.54	4.62
	tjx86b	5713	2.29	0.73	0.49	n.a.	1.83	1.69
	tjx87b	5718	2.21	0.61	0.38	n.a.	2.47	2.15
	average	9157	1.35	0.53	0.33	0.78	1.45	1.79
	s.e.m.	1889	0.15	0.03	0.02	0.08	0.13	0.23
CB+ dendrite-targeting	tjx21i	15392	0.92	0.55	0.33	0.57	1.35	0.39
	tjx22c	3866	1.83	0.83	0.54	1.48	1.12	1.65
	tjx59b	2761	1.10	0.54	0.34	0.96	1.32	1.32
	average	7340	1.28	0.64	0.41	1.00	1.26	1.12
	s.e.m.	4039	0.28	0.10	0.07	0.26	0.07	0.38
AStria-projecting	tjx45a	5890	1.32	0.58	0.37	0.99	1.39	2.45
	tjx52a	7339	0.82	0.46	0.30	n.a.	2.94	1.07
	tjx68a	4722	1.28	0.58	0.39	n.a.	2.10	4.37
	tjx83c	3514	1.07	0.48	0.33	n.a.	1.90	2.47
	average	5366	1.12	0.52	0.35	0.99	2.08	2.59
s.e.m.	817	0.11	0.03	0.02	n.a.	0.32	0.68	
Principal neurons	tjx25e	601	1.59	0.74	0.46	1.21	1.37	0.97
	tjx47b	3785	1.79	0.96	0.65	1.52	1.26	1.56
	tjx72c	965	3.23	1.02	0.57	n.a.	2.04	4.97
	tjx73a	1045	2.50	0.95	0.63	n.a.	1.32	8.39
	tjx73b	1504	1.96	1.07	0.68	1.39	1.15	2.74
	tjx75a	732	2.21	1.18	0.79	1.63	1.35	3.98
	tjx75b	704	3.25	1.52	1.08	n.a.	1.77	2.38
	tjx77b	256	2.01	1.08	0.73	1.26	2.19	2.15
	tjx79a	619	2.92	1.12	0.81	n.a.	1.85	2.88
	tjx79b	528	2.61	1.16	0.85	1.84	1.69	3.51
	tjx81a	199	2.04	1.07	0.73	1.66	1.98	2.15
	tjx81c	1246	1.91	0.98	0.65	1.48	1.67	2.24
	tjx82a	280	2.27	1.17	0.81	1.81	1.60	1.89
	tjx82b	2001	2.18	1.09	0.68	1.63	1.57	1.55
	tjx83b	325	1.64	0.97	0.63	1.09	1.39	2.19
	tjx84b	768	2.64	1.00	0.72	n.a.	2.75	3.51
	tjx84c	196	2.72	1.20	0.85	1.93	1.64	2.72
	tjx86c	2033	1.51	0.90	0.62	0.93	1.80	1.98
	tjx88a	1860	1.59	0.95	0.63	1.19	1.48	3.21
	tjx88b	334	2.86	1.36	0.98	0.00	1.84	2.68
	tjx89a	1214	1.53	0.89	0.60	1.09	1.75	1.25
	tjx89b	641	1.87	0.97	0.62	1.49	1.51	1.38
	tjx89c	2172	1.85	0.98	0.68	1.26	1.98	3.28
average	1044	2.20	1.06	0.71	1.36	1.69	2.76	
s.e.m.	180	0.11	0.03	0.03	0.10	0.07	0.32	

Table S5. Spike waveform parameters of all GABAergic and principal neurons.

All spike duration parameters were smaller for interneurons ($p < 0.0001$, Mann-Whitney U-test), except trough-2nd peak duration,. The 1st peak/trough amplitude ratio did not differ between interneurons and principal cells ($p > 0.1$, Mann-Whitney U-test); See Figure S8A for cursor names (c1 to c5, a1 and a2). n.a.: not applicable.

BLA recording	Ventral HPC reference					Dorsal CA1 reference		
	Cell code	Electrode location	Distance to str. pyramidale (μm)	Preferred theta phase (degrees)	Modulation depth	p (Rayleigh test)	Preferred theta phase (degrees)	Modulation depth
tx87b (PV+ basket)	vCA1 (str. radiatum)	355.00	62.2	0.03	1.1×10^{-2}	183.5	0.04	5.7×10^{-9}
tjx88a (principal cell)	vSubiculum (str. radiatum)	450.00	329.3	0.06	4.9×10^{-2}	n.s.	n.s.	5.8×10^{-2}
tjx88b (principal cell)	vSubiculum (str. radiatum)	450.00	n.s.	n.s.	2.1×10^{-1}	n.s.	n.s.	1.9×10^{-1}
tjx89a (principal cell)	vSubiculum (str. radiatum)	360.00	196.5	0.13	4.6×10^{-7}	268.2	0.12	3.1×10^{-7}
tjx89b (principal cell)	vSubiculum (str. radiatum)	360.00	124.4	0.07	4.1×10^{-2}	176.1	0.09	3.0×10^{-3}
tjx89c (principal cell)	vSubiculum (str. radiatum)	360.00	117.3	0.17	2.9×10^{-7}	213.7	0.19	9.4×10^{-10}

Recording	Phase differences (degrees)	
	Neuron phase difference (dCA1 - vCA1)	LFP phase difference
tx87b	121.3	101.2
tjx88a	n.a.	32.9
tjx88b	n.a.	39.0
tjx89a	71.6	59.8
tjx89b	51.7	55.7
tjx89c	96.45	78.0

Table S6. Theta phase modulation of BLA neuron firing assessed with dorsal and ventral hippocampal references. n.a.: not applicable; n.s.: not statistically significant.

Molecule	Species	Provider	Code / Catalogue number	Dilution	Specificity
Ankyrin G	Mouse	UC Davis/NIH NeuroMab Facility	75-146 (clone N106/36)	1:2,000-1:4,000	Manufacturer informations and labels axon initial segments and Ranvier nodes, as published with other antibodies.
Calbindin	Mouse	Swant	300	1:250-400	(Celio, 1990)
	Rabbit	Swant	CB38	1:5,000	(Airaksinen et al., 1997) and manufacturer informations.
CaMKII α	Mouse	Abcam	ab22609 (clone 6G9)	1:500	(Erondu and Kennedy, 1985)
Calretinin	Goat	Swant	CG1	1:1,000-2,000	Manufacturer informations and labeling pattern as published with other antibodies.
CB1-R	Guinea Pig	Dr. M. Watanabe, Hokkaido University	-	314 ng.mL ⁻¹	(Fukudome et al., 2004)
DARPP-32	Mouse	Prof. Drs. P. Greengard and A. Nairn	Clone D32 6a	1:250	(Hemmings and Greengard, 1986; Ouimet et al., 1984)
	Rabbit	Cell Signaling Technology	2302	1:200	(Partida et al., 2004)
GABA _A -R α 1	Rabbit	Prof. Dr. J.M. Fritschy, University of Zurich	-	1:10,000	(Benke et al., 1991)
GAD	Mouse	Chemicon/Millipore	MAB351R, (clone GAD-6)	1:500	(Chang and Gottlieb, 1988)
Kv 3.2	Rabbit	Alomone	APC-011	1:500	(McDonald and Mascagni, 2006) and manufacturer information.
Nk1-R	Guinea pig	Chemicon/Millipore	AB5800	1:700	Manufacturer information and labeling pattern as published with other antibodies.
Parvalbumin	Guinea pig	Synaptic systems	195-004	1:2,500-5000	Labeling pattern as published with other antibodies.
	Goat	Swant	PVG-214	1:2,000	Manufacturer information and labeling pattern as published with other antibodies.
Somatostatin	Mouse	GeneTex	GTX7 1935 (clone SOM-018)	1:250	Manufacturer information and labeling pattern as published with other antibodies.
VGAT	Rabbit	Synaptic systems	131-003	1:500	Manufacturer information and labeling pattern as published with other antibodies.
VGluT1	Mouse	Synaptic systems	135-311	1:500	Manufacturer information and labeling pattern as published with other antibodies.

Table S7. Primary antibodies used.

CaMKII α : Calcium/calmodulin dependant kinase II alpha subunit, CB1-R: cannabinoid receptor 1, DARPP-32: dopamine and cyclic adenosine 3', 5'-monophosphate-regulated phosphoprotein with molecular weight of 32 kDa, GAD: glutamic acid decarboxylase, Nk1-R: neurokinin receptor 1, VGAT: vesicular GABA transporter, VGluT1: vesicular glutamate transporter 1.

SUPPLEMENTAL EXPERIMENTAL PROCEDURES

Principal cells: recordings and analysis

Recordings were obtained as described for GABAergic cells in the main text, from 15 of the 70 rats used in the study. Recordings lasted 75 ± 42 min (mean \pm s.d., range 19-183 min) and yielded 175-3,172 spikes during dCA1 theta oscillations. Owing to the firing activities of principal neurons, their firing rates and coefficients of variation were calculated over time periods containing 50 spikes (same periods for firing rate and CV). Cells were confirmed as glutamatergic principal neurons if they expressed the vesicular glutamate transporter 1 (VGluT1) in axon varicosities. We also tested immunoreactivity for CaMKII α and calbindin.

Anatomically-identified principal cells fired wide spikes at low rates, with frequent spike bursts. Five putative (unlabeled) principal neurons were included for analysis based on this clear electrophysiological signature: broad spikes, low firing rates and occurrence of spike bursts. Their firing patterns and spike features were not different from that of identified neurons (see Table S4 and Figure S8).

The mean firing rate of all BLA principal cells studied here was 0.29 Hz, which is higher than that reported in an unbiased study of BLA projection cells' firing (0.09 Hz) (Gaudreau and Pare, 1996), but lower than reported using techniques based on spike sorting of spontaneously active units (~2 Hz) (Herry et al., 2008). By slowly ($\sim 1 \mu\text{m}\cdot\text{s}^{-1}$) advancing the recording electrode, we did not bias our recordings towards the most active principal cells. However, only spontaneously firing (but not silent cells) are recorded extracellularly. In addition, our phase analysis required at least 100 spikes to have occurred during hippocampal theta periods. Cells silent during these epochs were therefore excluded.

Only one principal cell in our sample fired at a rate above 1 Hz, indicating that neurons with spontaneous firing rate > 1 Hz are almost exclusively GABAergic interneurons. Moreover, all the neurons labeled when our recordings were biased towards units with large action potentials, burst firing and low firing frequencies were confirmed to be glutamatergic neurons. These data suggest that firing rates and spike features (see above) can be used in combination to reliably distinguish interneurons from principal neurons recorded extracellularly.

All confirmed BLA glutamatergic neurons (expressing VGluT1) also expressed CaMKII α (n= 14/14 tested, Table S4). In the BLA, CaMKII α thus appears to be a specific (McDonald et al., 2002) and sensitive (the present result) marker of glutamatergic principal neurons. This validates our method of interneurons' postsynaptic target identification at light and electron microscopy levels. Calbindin (CB) is expressed in a subset of BLA principal neuron ((Kemppainen and Pitkanen, 2000; McDonald, 1997), 12/18 here). Of the electrophysiological parameters we studied (Table S4), only CV differed between CB+ and CB- neurons. Calbindin-negative principal neurons had higher CVs (CB- vs. CB+, mean 2.5 vs. 1.9, unpaired t-test; p= 0.016), likely indicating that they generated more spike bursts. This result is consistent with stronger bursting activity in deep CA1 pyramidal cells ((Mizuseki et al., 2011), most of which are CB-) compared with superficial cells (most of which are CB+ (Baimbridge and Miller, 1982)).

Single principal cells electrophysiological and immunocytochemical data are summarized in Table S4.

Ventral hippocampal recordings and analysis

In 3 experiments, ventral hippocampal LFPs (vCA1-subiculum) were recorded with a glass electrode simultaneously with BLA, dCA1 and ECoG signals (recorded as stated in Experimental Procedures).

To reach the vCA1-subiculum, a medio-lateral 20° angle was used. Since theta phase gradually shifts in str. radiatum (Lubenov and Siapas, 2009), we initially aimed to record in str. pyramidale. The position of vCA1-subiculum str. pyramidale was identified online by the recording of several units within a short electrode trajectory (~100 μ m), which fired long-duration spikes and complex spike bursts. We found low amplitude, intermittent theta oscillations in str. pyramidale of vCA1-subiculum (Figure S9A). In str. radiatum, theta oscillations were transient, but more frequent and of higher amplitude than those in str. pyramidale (Figure S9B). These differences are reflected in the corresponding power spectra (Figure S9C). Therefore, str. radiatum LFP signal was used as a second reference.

At the end of the experiment, a Neurobiotin deposit was made (see Experimental Procedures) in str. pyramidale. Str. radiatum recording locations (as shown in Figure S9D and Figure 7E) were extrapolated from the electrode trajectories and the documented distances to the Neurobiotin deposits in str. pyramidale.

Power spectra as illustrated in Figure S9C were obtained as follows. After applying a 0.5 Hz high pass filter, fast Fourier transforms of LFPs were computed over 200 s of robust dCA1 theta oscillations. Data were windowed with a Hanning filter (0.1995 Hz windows) and power spectra were constructed (Spike2).

Neuron firing relations to ventral hippocampal theta were computed from the same time periods as for dCA1 theta analysis. This allowed for the comparison between preferred phases computed with the two references. Statistical significance threshold of Rayleigh's test was reduced to 0.05 for analysis of BLA neuron modulation by ventral hippocampal theta.

Brains fixation and sectioning

The animals were given a lethal dose of ketamine 30 min to 4 h after juxtacellular labeling, and perfused via the ascending aorta with ~60 mL of Phosphate Buffer Saline (PBS, pH 7.4), followed by 300 mL of fixative containing 4% w/v paraformaldehyde, 0.1% v/v glutaraldehyde, 15% v/v saturated picric acid, in PB 0.1 M, pH~7.3 (100 mL at 20 mL.min⁻¹ then 200 mL at 10 mL.min⁻¹). Brains were dissected out and stored overnight in PBS. They were cut in 60 µm-thick coronal sections with a vibrating microtome (Leica VT-1000), extensively washed in PBS, and conserved in PB 0.1 M with 0.05% NaN₃ until use.

Immunofluorescence: Neurobiotin-filled neurons were visualized with streptavidin conjugated to a fluorophore, then tested for their neurochemical content using immunofluorescence. All reagents were diluted in PBS containing 0.15% v/v triton X-100. Free-floating sections were blocked in 20% normal horse serum (NHS, Vector laboratories) for 1h at room temperature and incubated at 4°C for 2 days in one or several primary antibodies with 2% NHS (antibodies listed in Table S7, with references showing their specificity). Sections were washed, and incubated at 4°C overnight with appropriate highly cross-adsorbed secondary antibodies, coupled to Cy3, Cy5, Dylight 405 (Jackson ImmunoResearch Laboratories) or Alexa 488 (Invitrogen), with 2% NHS. After several washes, sections were mounted in Vectashield (Vector Laboratories).

Immunoreactivity was evaluated using epifluorescence (Leica DMRB microscope fitted with a 40x 0.7 NA objective), structured illumination (Apotome system operated with Axiovision software) and confocal microscopy (LSM 710

operated with Zen 2008 software) with a AxioImager Z1 microscope fitted with 40x NA 1.3 and 63x NA 1.4 oil objectives (hardware and software from Carl Zeiss Ltd.). For confocal imaging, single-channel sequential frame scanning was used to avoid crosstalk. Pinhole size was adjusted to preserve a constant optical slice thickness across channels (typically 1.1 μm for 40x, 0.7 μm for 63x). Beam splitter and wavelength acquisition bands were adjusted using the “Smart” function of Zen software. Wavelength acquisition bands were occasionally narrowed to avoid acquiring signal resulting from excitation crosstalk. Optimal pixel size was set using the built-in function of Zen and kept constant for all channels.

Absence of crosstalk was ensured by absence of “copy” of one channel in another in the section analyzed and in a single-stained control sample. A neuron was concluded immunopositive if the staining pattern was as expected, crosstalk excluded and co-localization evident with the relevant compartments of the streptavidin-labeled neuron. If no colocalization was observed, the neuron was concluded negative. If the staining was suboptimal or crosstalk persisted, the cell was listed as not tested. Brightness and contrast were adjusted for entire image frames using Photoshop (Adobe CS3).

Preferred postsynaptic targets (putative) were determined qualitatively with fluorescence and/or transmission light microscopy. A majority of axon varicosities making close appositions with CaMKII α + somata and large calibre dendrites in the BLA indicated the neuron was a basket cell. A majority of appositions with ankyrin G+ axon initial segments (AIS) defined the cell as axo-axonic (Gulyas et al., 2010). When the axon made apposition with CaMKII α + dendrites and with non-apparent structures (potentially too small for detection with light microscopy), the cell was classified as dendrite-targeting.

Electron microscopy was used to validate light microscopic observations and to evaluate quantitatively postsynaptic target preference. Indeed, light microscopy gives an estimate of preferred targets but can be inaccurate in quantifying their relative proportions (Tamas et al., 1997).

Sections were cryoprotected with 20% w/v sucrose in PB 0.1 M and freeze-thawed over liquid nitrogen to enhance penetration of reagents. Sections were then incubated with a streptavidin-biotinylated horseradish peroxidase (HRP) complex (ABC Elite kit, Vector Laboratories) and Neurobiotin-filled cells were visualised with

HRP reaction products using nickel-intensified diaminobenzidine (DAB) as a chromogen. Postsynaptic profiles belonging to principal neurons were identified at electron microscopic level with an immunoperoxidase method against CaMKII α . Sections were blocked in 20% normal goat serum (NGS, Vector laboratories) for 1h at room temperature, incubated at 4°C for 2 days in 1:500 mouse anti-CaMKII α (Table S7) in PB 0.1 M NGS 2%. Sections were washed and incubated overnight at 4°C with a HRP-coupled goat anti-mouse antibody (Dako) diluted 1:100 in PB 0.1 M with NGS 2%. Sections were washed and reacted with non-intensified DAB.

Sections were postfixated with 1% OsO₄ (TAAB Laboratory Equipment; in PB 0.1 M), block-stained in 1% uranyl acetate (TAAB), dehydrated, embedded in epoxy resin (Durcupan; Fluka) and mounted on glass slides. Axon-rich areas were cut out and re-embedded in resin. Serial ultrathin sections (70 nm) were cut with an ultramicrotome (Ultracut S; Leica) and collected on Pioloform-coated copper slot grids.

Analysis of the specimens was performed using a Philips CM 120 electron microscope. Axons were examined for the identity of postsynaptic targets without further contrasting. Sampling randomization was achieved as follows: blocks were cut out from random axon-rich areas and all axon profiles were followed and analyzed until 20 synapses were collected. In some instances, our analysis yielded additional synapses, which were also included for quantification. Postsynaptic targets were always followed in serial sections. Their identity was determined using standard criteria (Peters et al., 1991). When the target was a dendrite, its diameter (defined as its smaller axis) was measured. In sections where CaMKII α was stained with DAB, clear DAB-labeled structures were considered as part of glutamatergic neurons. Because in our samples many small dendrites and dendritic spines were not labeled, we did not conclude on the identity of structures in which HRP product was not detected.

Camera lucida reconstructions of neurons were performed using a drawing tube mounted onto a Zeiss Axioplan2 microscope with a 63x oil 1.4 NA objective. Amygdala nuclei boundaries were drawn from one of the 2 sections from which the axon was reconstructed. We used adjacent coronal sections and, in several instances immunohistochemistry, to determine boundaries between lateral and basal amygdala nuclei.

Modulation of BLA interneuron's firing by CA1 gamma oscillations

Neuronal spiking modulation with dCA1 gamma oscillation was assessed according to the method published in Tukker et al. (2007), using the same custom Spike2 analysis program.

LFPs recorded in dCA1 were digitally low pass-filtered (300 Hz) off-line. LFPs were then down-sampled to 1 kHz and digitally filtered to extract gamma oscillations (bandpass 30–80 Hz Finite Impulse Response filter). For firing modulation analysis, we selected the gamma cycles with amplitude greater than the mean amplitude calculated over the entire duration of the recording. Two types of gamma oscillation epochs were analyzed: those occurring specifically during theta oscillations (epochs as defined in Experimental Procedures), and those occurring indifferently throughout the recording.

Gamma oscillation troughs were detected and gamma cycle angles were linearly interpolated between consecutive troughs. Rayleigh's test was used to assess modulation of individual neurons in phase with dCA1 gamma (significance threshold $p=0.005$; more details on Rayleigh's test can be found in Experimental Procedures).

Extracellular spike waveform analysis

For all interneurons ($n=28$) and principal cells ($n=23$), extracellular spikes detected during theta oscillations (see Experimental Procedures for theta epochs detection) were averaged from the BLA "unit" channel (300-5000 Hz filter). The event-triggered averaging function of Spike 2 was applied offline, using spike time stamps as a trigger.

On these averaged spike waveforms, reference cursors were placed as follows: c1 at the start of the first positive deflection, c2 at the first peak, c3 at the trough, c4 when the spike reached baseline again, c5 at the second peak (Figure S8A). Five parameters were measured and compared across cell classes. Four spike duration values: total width (c1-c4), baseline to trough (c1-c3), first peak to trough (c2-c3), trough to second peak duration (c3-c5); one amplitude parameter: the 1st peak / trough amplitude ratio. In some cells, it was not possible to determine the last parameter of spike duration due to the lack of second peak. In addition to these, spike amplitude was measured from 1st positive peak to trough.

Kruskal Wallis test was used to compare values across interneuron types. Mann-Whitney U-test was used to compare values measured in interneurons versus principal cells. Unsupervised hierarchical cluster analysis was performed to further investigate

whether cell types could be separated on the basis of their spike waveforms. Two parameters were included: the 1st peak to trough duration (c2-c3) and the 1st peak/trough amplitude ratio (a1/a2). Clustering was performed using the Euclidean distance followed by the minimum variance ward algorithm embedded in Matlab (MathWorks). The lowest (> 1) number of final clusters was determined as the one that provided a robust inconsistency coefficient value.

SUPPLEMENTAL REFERENCES

Airaksinen, M.S., Eilers, J., Garaschuk, O., Thoenen, H., Konnerth, A., and Meyer, M. (1997). Ataxia and altered dendritic calcium signaling in mice carrying a targeted null mutation of the calbindin D28k gene. *Proc Natl Acad Sci U S A* 94, 1488-1493.

Baimbridge, K.G., and Miller, J.J. (1982). Immunohistochemical localization of calcium-binding protein in the cerebellum, hippocampal formation and olfactory bulb of the rat. *Brain Res* 245, 223-229.

Benke, D., Cicin-Sain, A., Mertens, S., and Mohler, H. (1991). Immunochemical identification of the alpha 1- and alpha 3-subunits of the GABAA-receptor in rat brain. *J Recept Res* 11, 407-424.

Celio, M.R. (1990). Calbindin D-28k and parvalbumin in the rat nervous system. *Neuroscience* 35, 375-475.

Chang, Y.C., and Gottlieb, D.I. (1988). Characterization of the proteins purified with monoclonal antibodies to glutamic acid decarboxylase. *J Neurosci* 8, 2123-2130.

Erondu, N.E., and Kennedy, M.B. (1985). Regional distribution of type II Ca²⁺/calmodulin-dependent protein kinase in rat brain. *J Neurosci* 5, 3270-3277.

Fukudome, Y., Ohno-Shosaku, T., Matsui, M., Omori, Y., Fukaya, M., Tsubokawa, H., Taketo, M.M., Watanabe, M., Manabe, T., and Kano, M. (2004). Two distinct classes of muscarinic action on hippocampal inhibitory synapses: M2-mediated direct suppression and M1/M3-mediated indirect suppression through endocannabinoid signalling. *Eur J Neurosci* 19, 2682-2692.

Gaudreau, H., and Pare, D. (1996). Projection neurons of the lateral amygdaloid nucleus are virtually silent throughout the sleep--waking cycle. *J Neurophysiol* 75, 1301-1305.

Gulyas, A.I., Szabo, G.G., Ulbert, I., Holderith, N., Monyer, H., Erdelyi, F., Szabo, G., Freund, T.F., and Hajos, N. (2010). Parvalbumin-containing fast-spiking basket cells generate the field potential oscillations induced by cholinergic receptor activation in the hippocampus. *J Neurosci* 30, 15134-15145.

- Hemmings, H.C., Jr., and Greengard, P. (1986). DARPP-32, a dopamine- and adenosine 3':5'-monophosphate-regulated phosphoprotein: regional, tissue, and phylogenetic distribution. *J Neurosci* 6, 1469-1481.
- Herry, C., Ciocchi, S., Senn, V., Demmou, L., Muller, C., and Luthi, A. (2008). Switching on and off fear by distinct neuronal circuits. *Nature* 454, 600-606.
- Kempainen, S., and Pitkanen, A. (2000). Distribution of parvalbumin, calretinin, and calbindin-D(28k) immunoreactivity in the rat amygdaloid complex and colocalization with gamma-aminobutyric acid. *J. Comp. Neurol.* 426, 441-467.
- Likhtik, E., Pelletier, J.G., Popescu, A.T., and Pare, D. (2006). Identification of basolateral amygdala projection cells and interneurons using extracellular recordings. *J Neurophysiol* 96, 3257-3265.
- Lubenov, E.V., and Siapas, A.G. (2009). Hippocampal theta oscillations are travelling waves. *Nature* 459, 534-539.
- Mallet, N., Pogosyan, A., Marton, L.F., Bolam, J.P., Brown, P., and Magill, P.J. (2008). Parkinsonian beta oscillations in the external globus pallidus and their relationship with subthalamic nucleus activity. *J Neurosci* 28, 14245-14258.
- McDonald, A.J. (1997). Calbindin-D28k immunoreactivity in the rat amygdala. *J. Comp. Neurol.* 383, 231-244.
- McDonald, A.J., and Betette, R.L. (2001). Parvalbumin-containing neurons in the rat basolateral amygdala: morphology and co-localization of Calbindin-D(28k). *Neuroscience* 102, 413-425.
- McDonald, A.J., and Mascagni, F. (2006). Differential expression of Kv3.1b and Kv3.2 potassium channel subunits in interneurons of the basolateral amygdala. *Neuroscience* 138, 537-547.
- McDonald, A.J., Muller, J.F., and Mascagni, F. (2002). GABAergic innervation of alpha type II calcium/calmodulin-dependent protein kinase immunoreactive pyramidal neurons in the rat basolateral amygdala. *J Comp Neurol* 446, 199-218.
- Mizuseki, K., Diba, K., Pastalkova, E., and Buzsaki, G. (2011). Hippocampal CA1 pyramidal cells form functionally distinct sublayers. *Nat Neurosci* 14, 1174-1181.
- Ouimet, C.C., Miller, P.E., Hemmings, H.C., Jr., Walaas, S.I., and Greengard, P. (1984). DARPP-32, a dopamine- and adenosine 3':5'-monophosphate-regulated phosphoprotein enriched in dopamine-innervated brain regions. III. Immunocytochemical localization. *J Neurosci* 4, 111-124.
- Partida, G.J., Lee, S.C., Haft-Candell, L., Nichols, G.S., and Ishida, A.T. (2004). DARPP-32-like immunoreactivity in AII amacrine cells of rat retina. *J Comp Neurol* 480, 251-263.
- Paxinos, G., and Watson, C. (2007). *The Rat Brain in Stereotaxic Coordinates*, 6th edition (Elsevier).

Peters, A., Palay, S.L. & Webster, H. deF. (1991). The fine structure of the nervous system, Oxford University Press.

Tamas, G., Buhl, E.H., and Somogyi, P. (1997). Fast IPSPs elicited via multiple synaptic release sites by different types of GABAergic neurone in the cat visual cortex. *J Physiol* 500 (Pt 3), 715-738.

Tukker, J.J., Fuentealba, P., Hartwich, K., Somogyi, P., and Klausberger, T. (2007). Cell type-specific tuning of hippocampal interneuron firing during gamma oscillations in vivo. *J Neurosci* 27, 8184-8189.